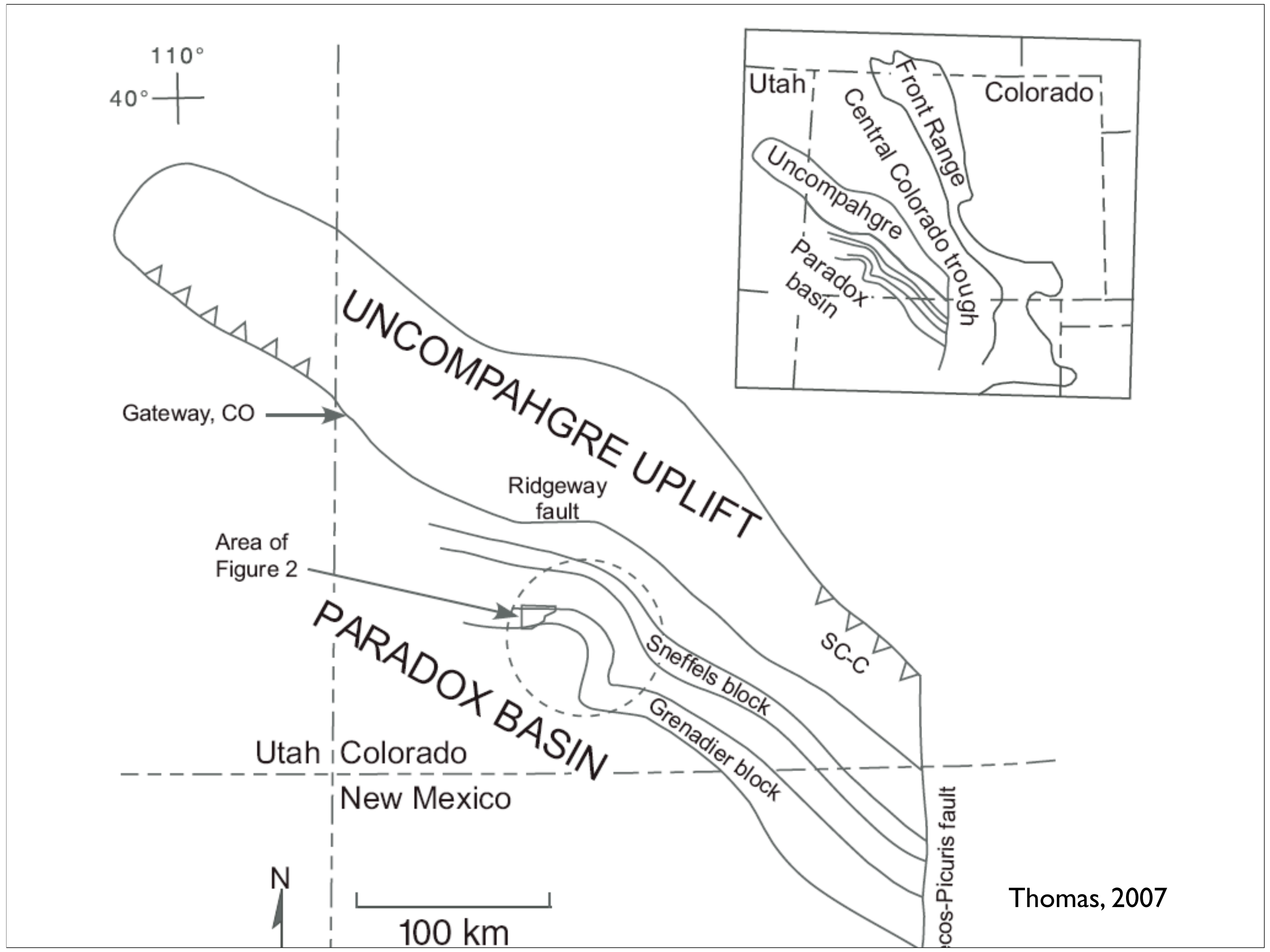
110°
40°
Utah
Colorado
Front Range
Central Colorado trough
Uncompahgre
Paradox basin
UNCOMPAHGRE UPLIFT
Gateway, CO
Ridgeway fault
Area of Figure 2
PARADOX BASIN
Sneffels block
Grenadier block
SC-C
Utah
Colorado
New Mexico
cos-Picuris fault
N
100 km

Thomas, 2007

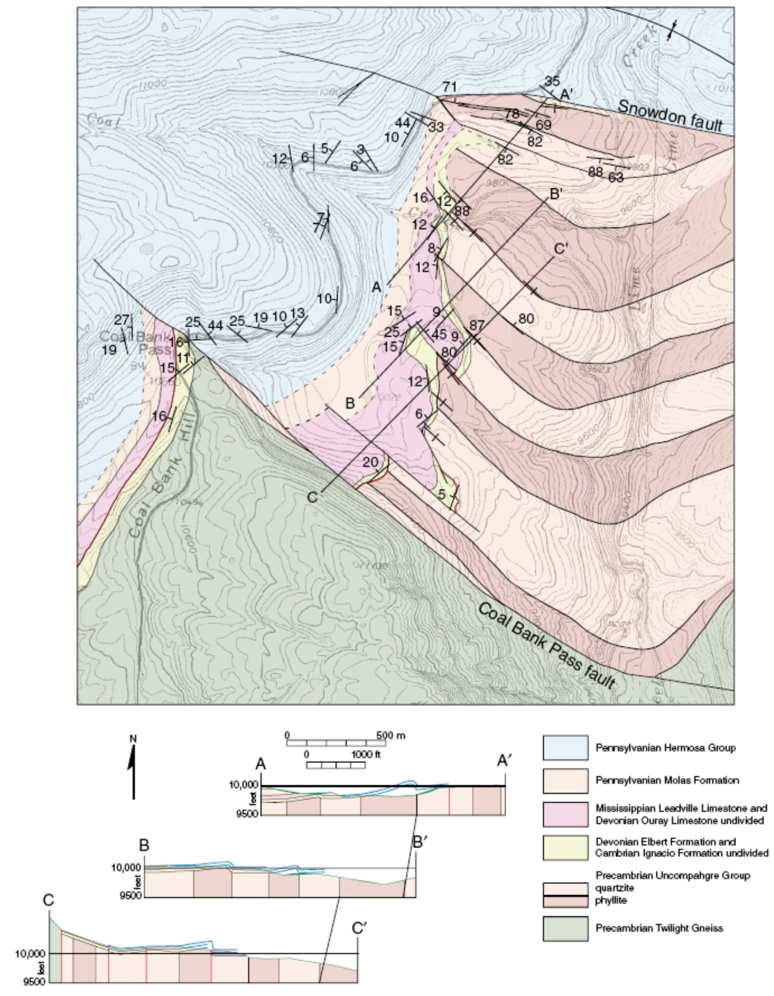
Snowdon fault
Coal Bank Pass fault
Coal Bank Pass
Coal Bank Hill
Pennsylvanian Hermosa Group
Pennsylvanian Molas Formation
Mississippian Leadville Limestone and Devonian Ouray Limestone undivided
Devonian Elbert Formation and Cambrian Ignacio Formation undivided
Precambrian Uncompahgre Group
quartzite
phyllite
Precambrian Twilight Gneiss
0 500 m
0 1000 ft
A
A′
B
B′
C
C′
10,000
9500
feet
N

Thomas, 2007

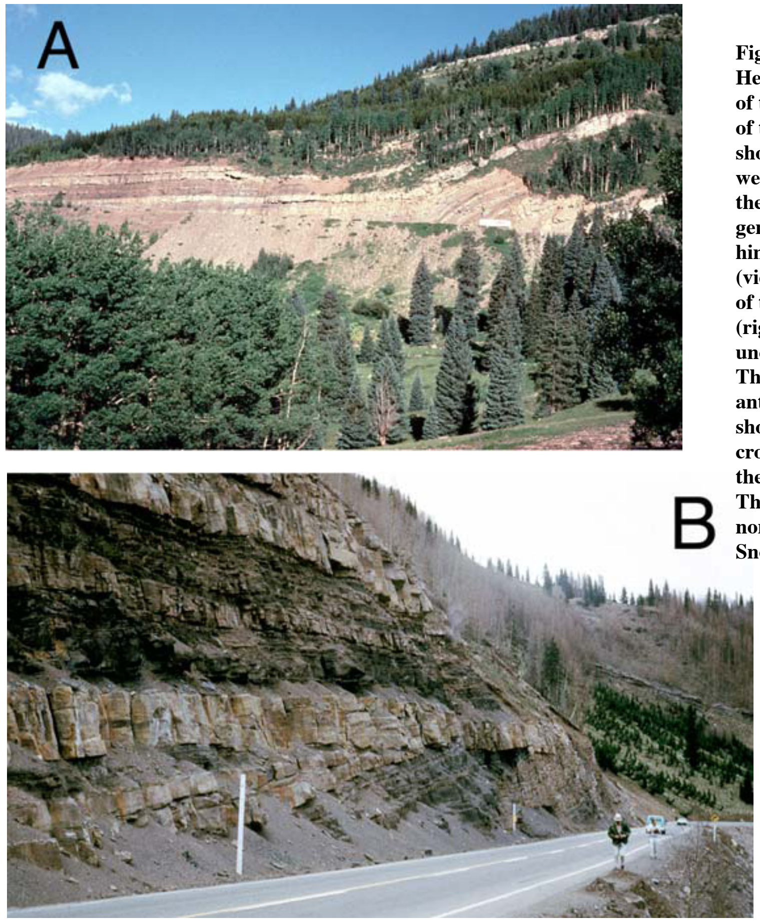

Figure 9. Photographs of angular unconformity in Hermosa beds exposed along U.S. Highway 550 south of the Snowdon fault. Orientations of the views are shown in Figure 2, and the location is shown in Figure 5. (A) Steep south limb of anticline at west end of the Snowdon fault; the angular unconformity is exposed beneath more gently dipping beds south (left in view) of the abrupt hinge on the south limb of the anticline (view to west). The crest of the anticline and the trace of the Snowdon fault are out of the view to the north (right in view). (B) Angular unconformity exposed in highway cut (view to north). The hinge and steep up-turn of the south limb of the anticline are hidden behind the shoulder of the highway cut. The Snowdon fault crosses the highway approximately at the position of the most distant car on the highway. The north-dipping beds in the distance are in the north limb of the anticline on the north side of the Snowdon fault.

Thomas, 2007

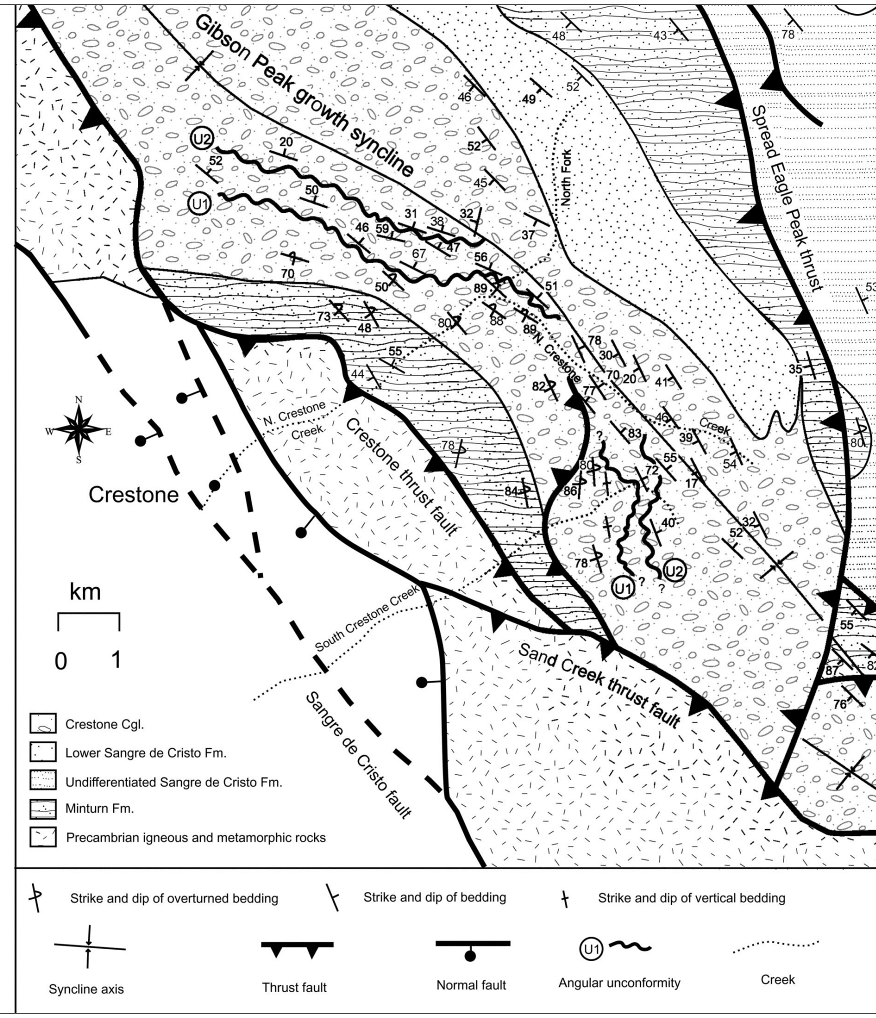

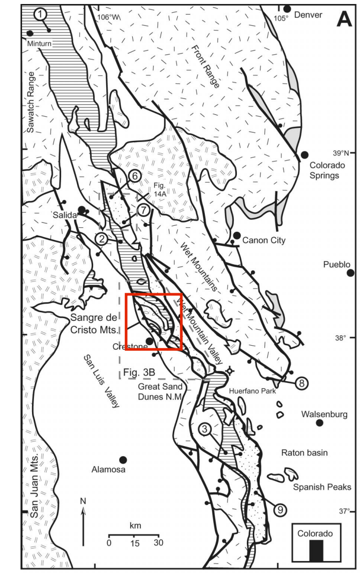

Hoy and Ridgway, GSA Bull, 2002

Growth structures in Sangres.

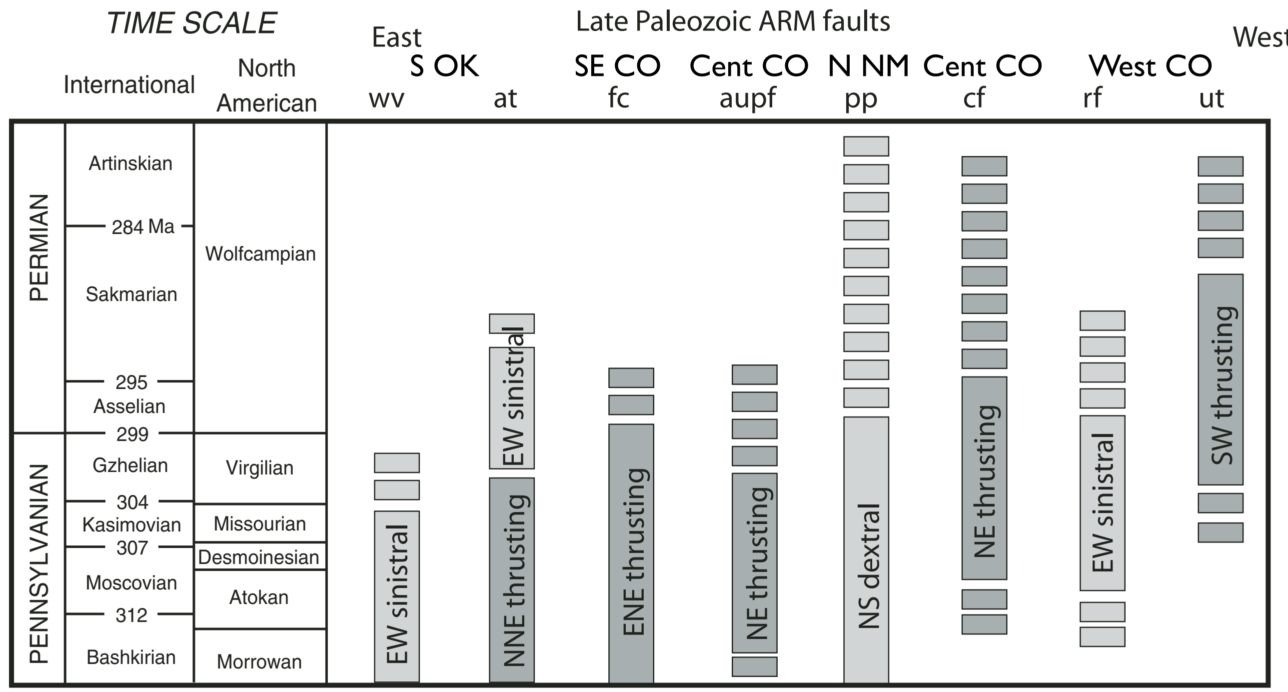

Figure 17. Inferred timing and kinematics of faults with a documented ancestral Rocky Mountains history. Light gray represents predominantly strike-slip motion, whereas dark gray indicates predominantly reverse motion. Dashed bars indicate range of time faulting is thought to have initiated (bottom of figure) or ceased (top of figure). Abbreviations: ut—Uncompahgre thrust (slip-sense from Frahme and Vaughn, 1983); rf—Ridgeway fault (slip-sense from Stevenson and Baars, 1986; Thomas, 2007); pp—Picuris-Pecos fault (slip-sense from Cather et al., 2006; Wawrzyniec et al., 2007); ct—Crestone thrust (slip-sense from Hoy and Ridgway, 2002); aupf—ancestral Ute Pass fault (slip-sense data herein); fc—Freezeout Creek fault (slip-sense from Maher, 1953; McKee, 1975); at—Anadarko thrust (slip-sense from Brewer et al., 1983); wv—Washita Valley fault (slip-sense from Tanner, 1967). Time scale is from Gradstein et al. (2004).

Sweet and Soreghan, GSA Bull 2009

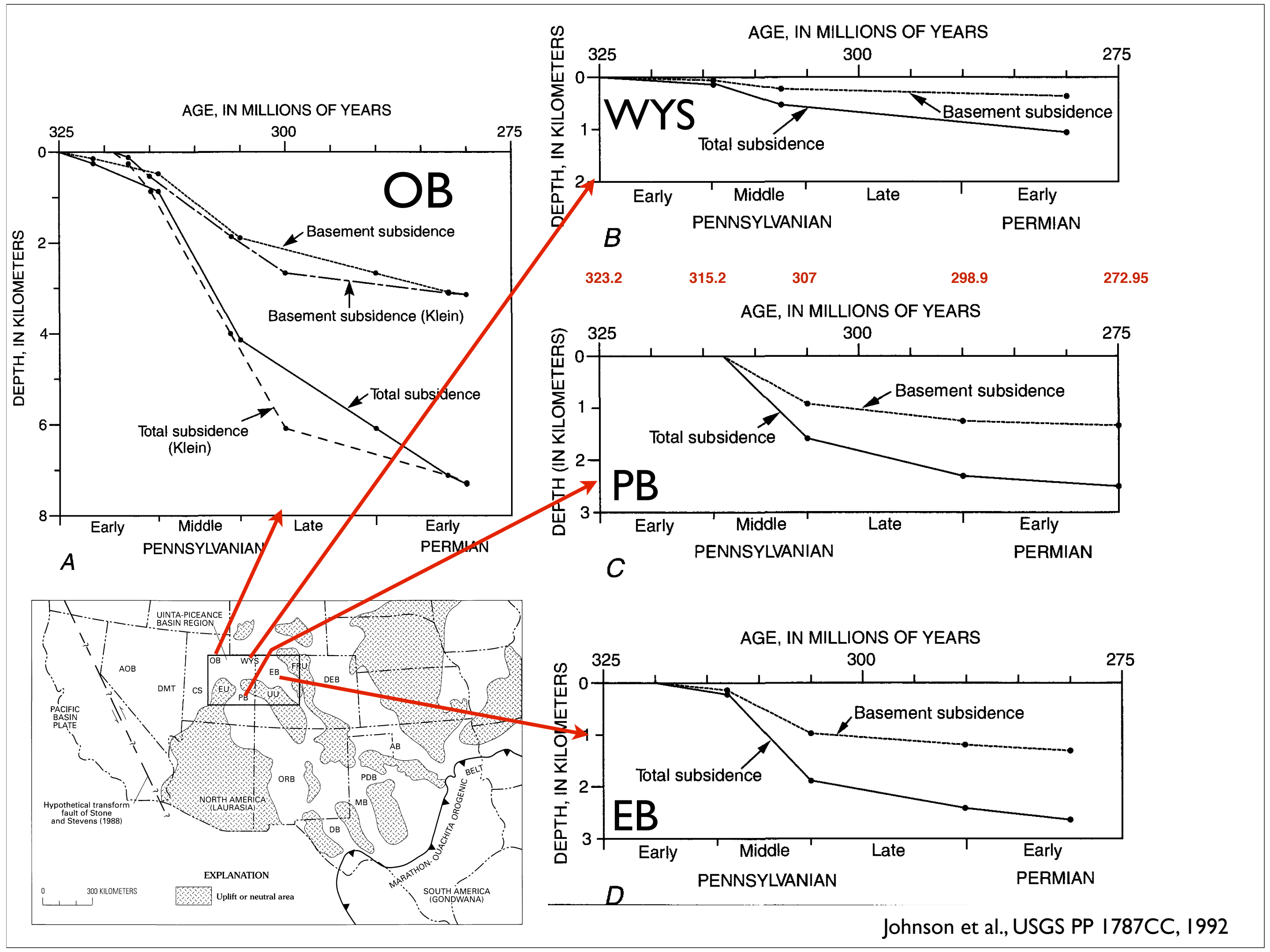

Note that this is with an older timescale, too.
Early Penn now 323.2–315.2
Middle 315.2–307
Late 307–298.9
Early Permian 298.9–272.95(?)

Tectonic Subsidence

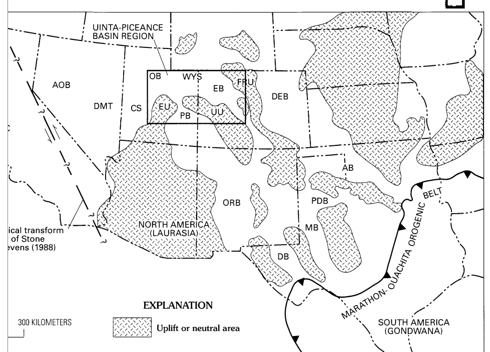

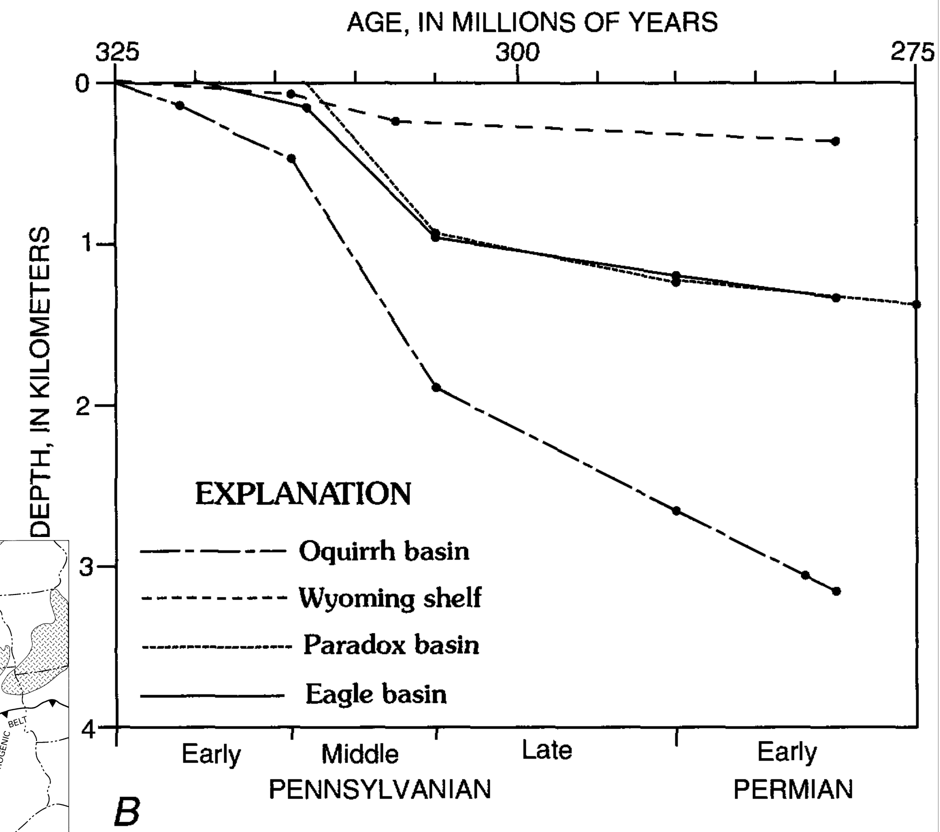

Johnson et al., USGS PP 1787CC, 1992

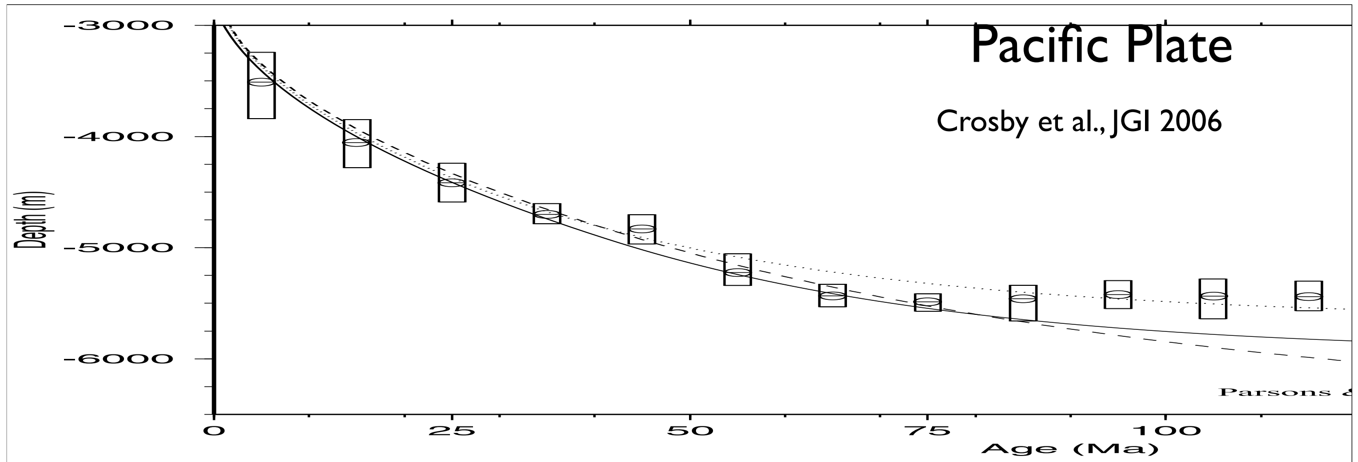

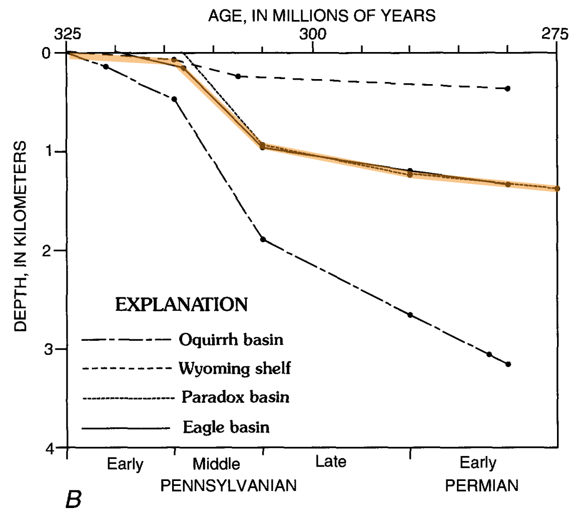

Johnson et al., USGS PP 1787CC, 1992

Pacific Plate

Crosby et al., JGI 2006

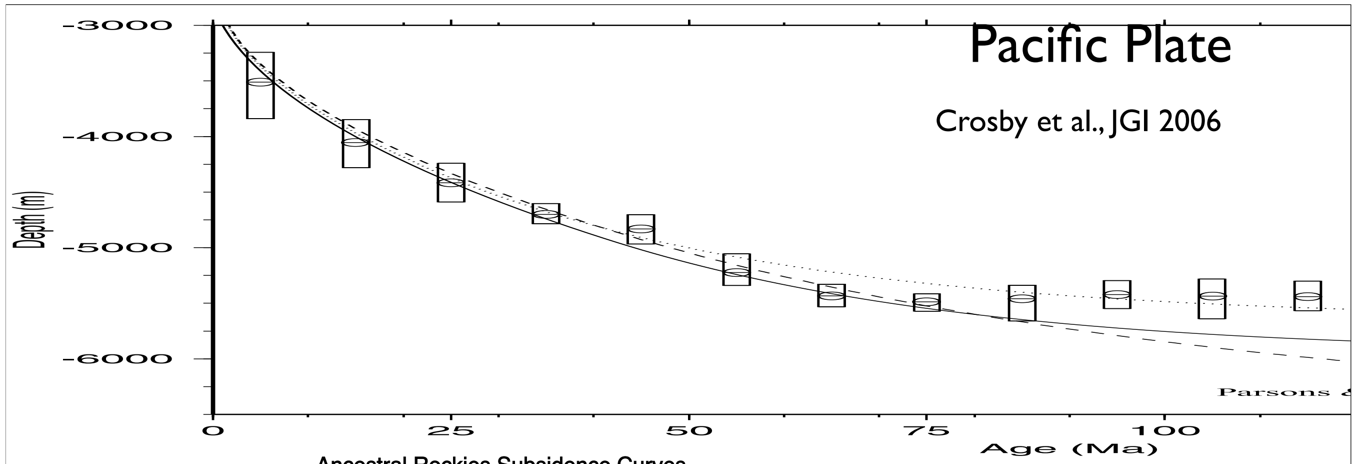

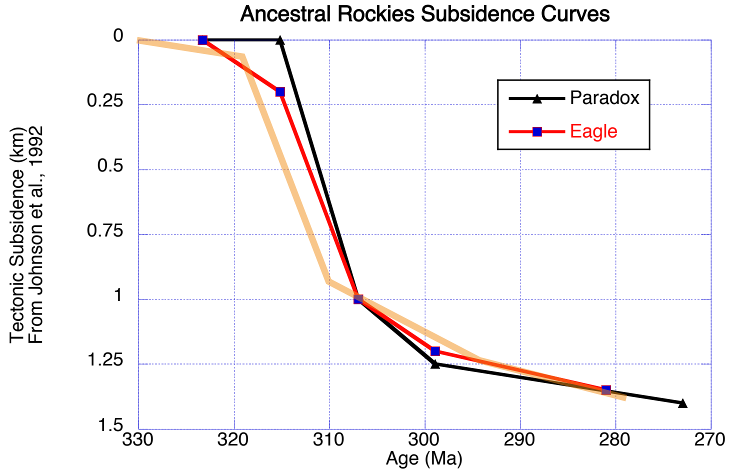

Updated timescale
(GSA v5, 2018)

Johnson et al., USGS PP 1787CC, 1992

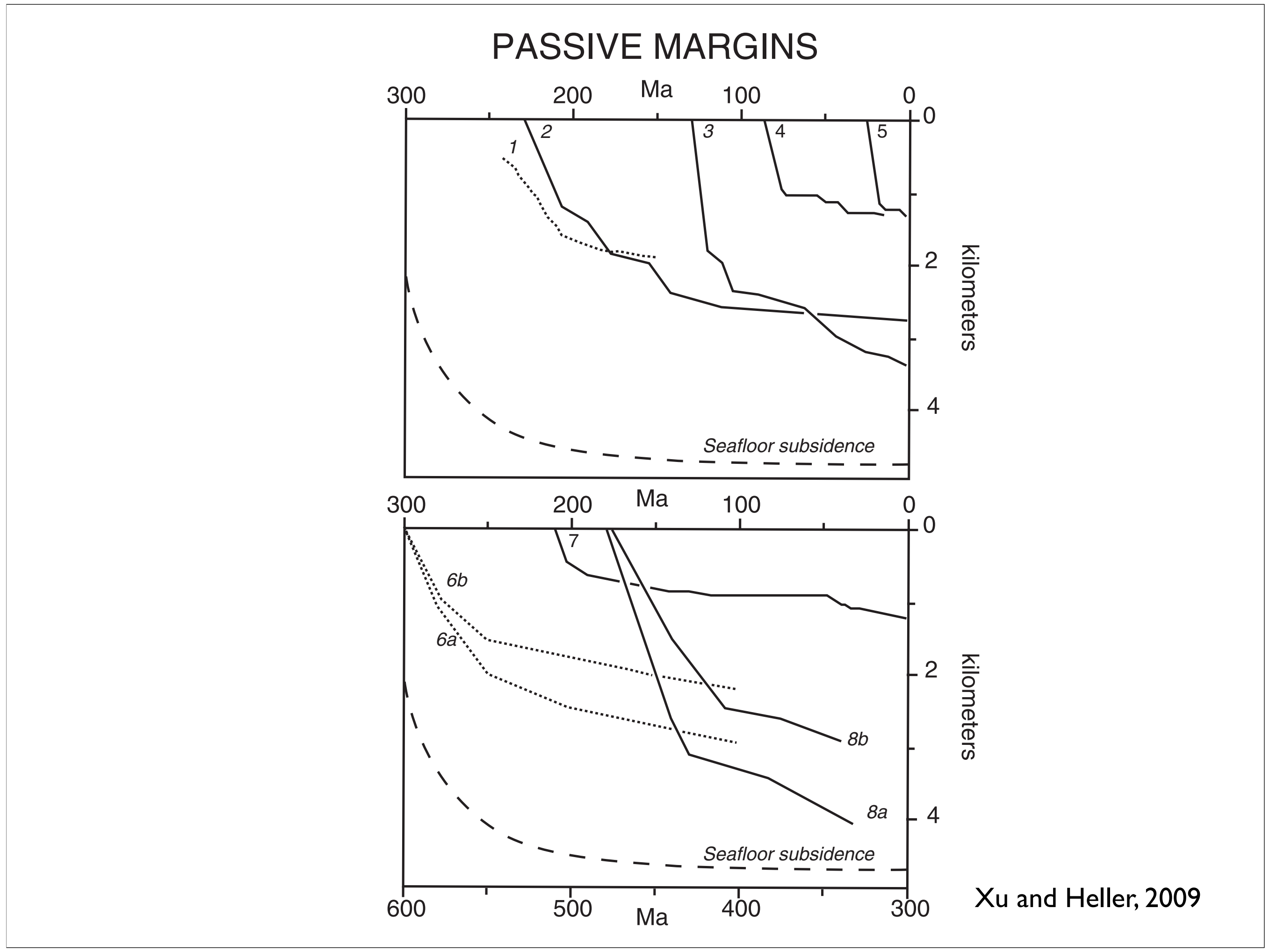

Figure 2. Tectonic subsidence curves for passive margin settings. Locations shown on Figure 1. Solid curves correspond to time scale at top of graph and dotted lines to time scale at bottom of graph. Thermal decay curve (dashed) for subsidence of cooling seafloor (Stein and Stein, 1992), minus (i.e., shallowed) 500 m, is shown for comparison. 1—Paleozoic Miogeocline, southern Canadian Rocky Mountains (Bond and Kominz, 1984); 2—Moroccan Basin (Ellouz et al., 2003); 3—Campos Basin (Mohriak et al., 1987); 4—Gippsland Basin (Falvey and Mutter, 1981; P. Yin, 1985, per- sonal commun.); 5—Gulf of Lion (Benedicto et al., 1996); 6—U.S. Cordilleran Miogeocline (Bissell, 1974; Armin and Mayer, 1983; Devlin et al., 1986; Devlin and Bond, 1988); 7—Lusitanian Basin (Stapel et al., 1996); 8—U.S. Atlantic margin (Steckler and Watts, 1978; Swift et al., 1987).

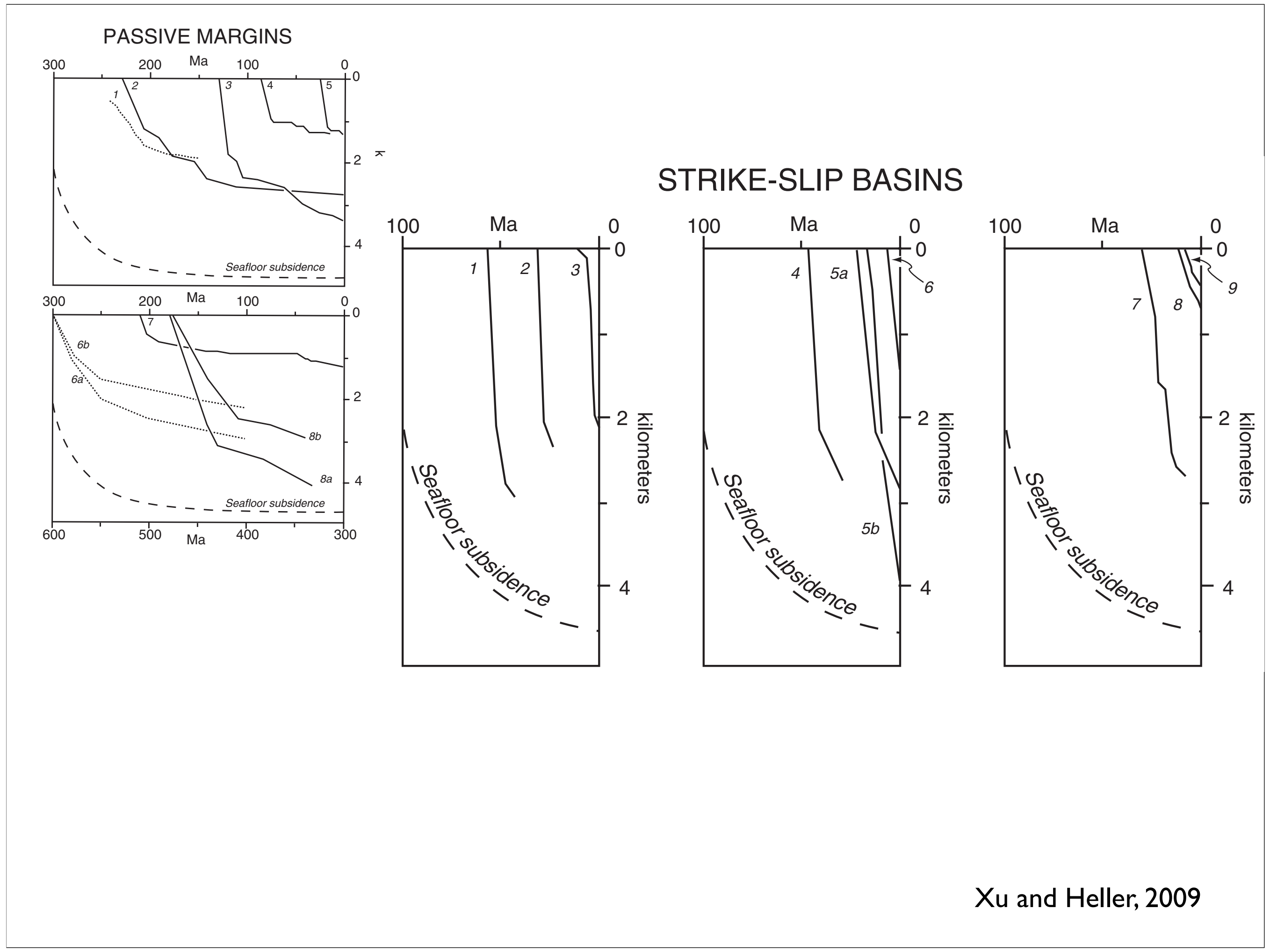

Figure 3. Tectonic subsidence curves for strike-slip basins. Locations shown in Figure 1. Thermal decay curve (dashed) for subsidence of cooling seafloor (Stein and Stein, 1992), minus 500 m, is shown for comparison. 1—Chuck- anut Basin (Johnson, 1984, 1985); 2—Ridge Basin (Crowell and Link, 1982; Karner and Dewey, 1986); 3—Death Valley (Hunt and Mabey, 1966); 4—Salinian block (Graham, 1976); 5—Los Angeles Basin (Rumelhart and Ingersoll, 1997); 6—Gulf of California (Curray and Moore, 1984); 7—Cuyama Basin (Dickinson et al., 1987); 8—Bozhang Depression (Hu et al., 2001); 9—Salton Trough (Kerr et al., 1979).

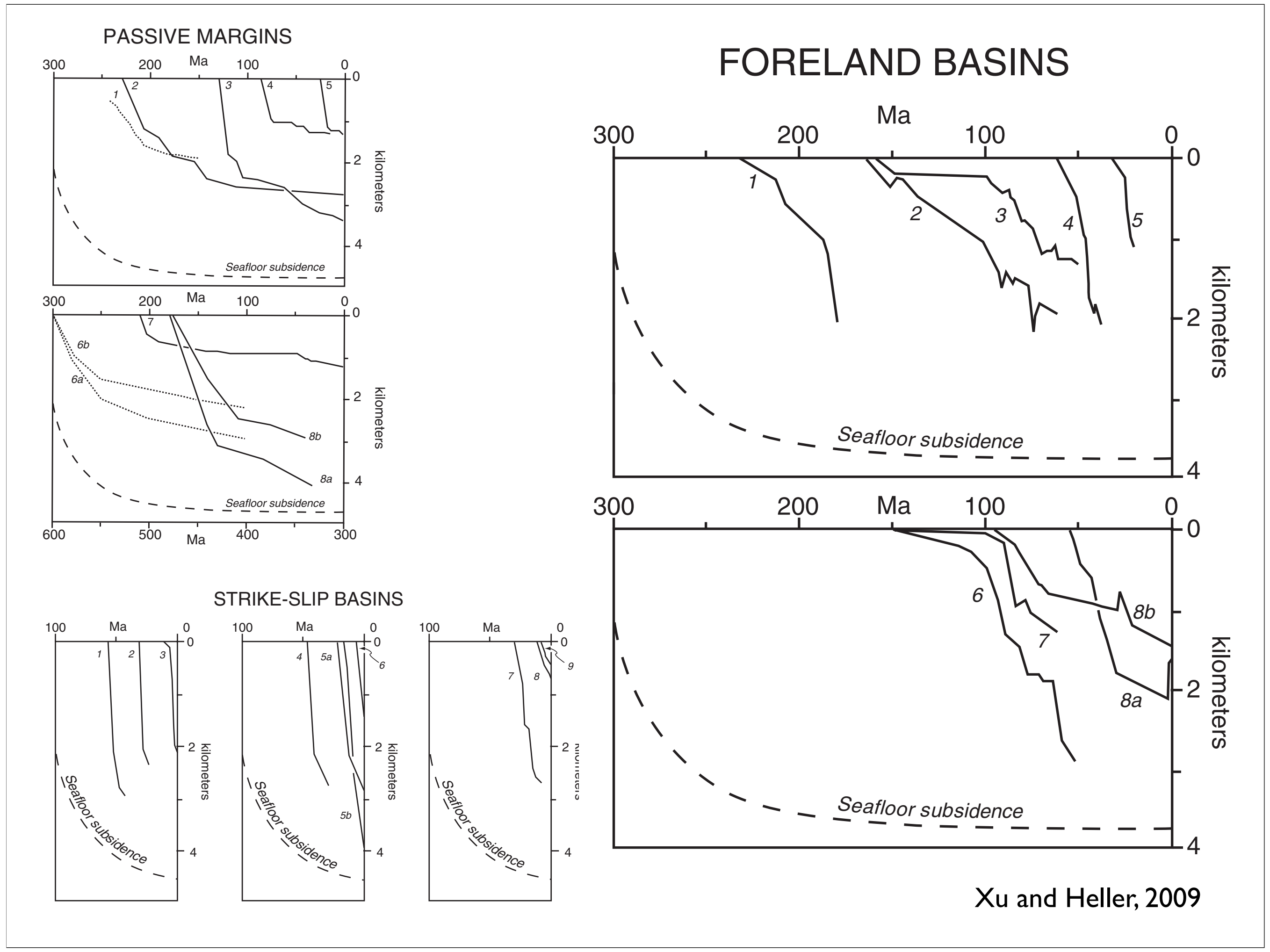

Figure 6. Tectonic subsidence of foreland basins. Locations shown in Figure 1. Thermal decay curve (dashed) for subsidence of cooling seafloor (Stein and Stein, 1992), minus 1500 m, is shown for comparison. 1—Eastern Avalonia, Anglo-Brabant fold belts (van Grootel et al., 1997); 2—Southern Alberta Basin (Gillespie and Heller, 1995); 3—San Rafael Swell, Utah (Heller et al., 1986); 4—Pyrenean foreland basin, Gombrèn (Vergés et al., 1998); 5—Swiss Molasse basin (Burkhard and Sommaruga, 1998) modified from total subsidence using water:sediment density contrast); 6—Hoback Basin, Wyoming (Cross, 1986); 7—Green River Basin, Wyoming (Cross, 1986; Heller et al., 1986); 8—Magallanes Basin (Biddle et al., 1986).

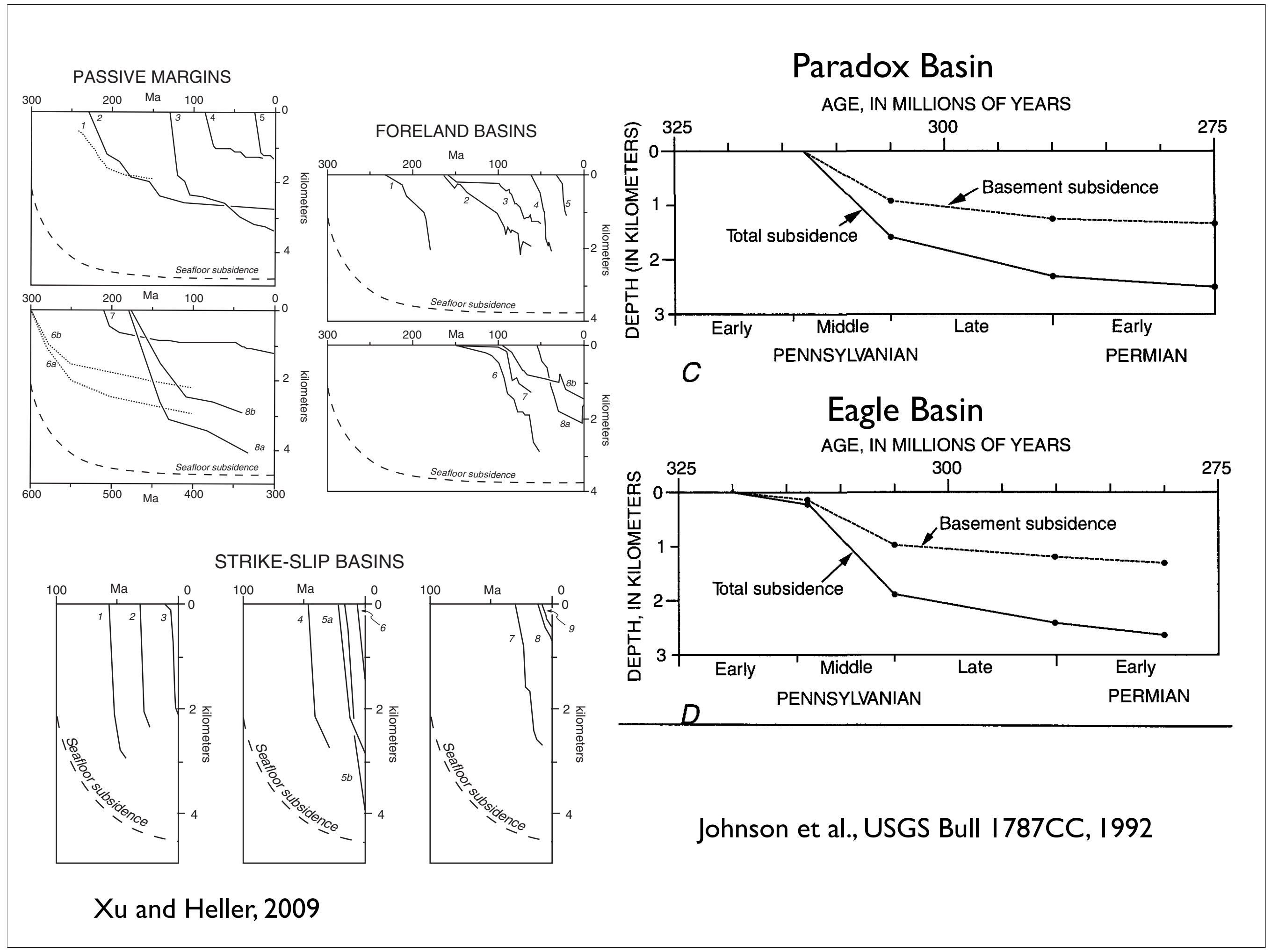

Figure 6. Tectonic subsidence of foreland basins. Locations shown in Figure 1. Thermal decay curve (dashed) for subsidence of cooling seafloor (Stein and Stein, 1992), minus 1500 m, is shown for comparison. 1—Eastern Avalonia, Anglo–Brabant fold belts (van Grootel et al., 1997); 2—Southern Alberta Basin (Gillespie and Heller, 1995); 3—San Rafael Swell, Utah (Heller et al., 1986); 4—Pyrenean foreland basin, Gombrèn (Vergés et al., 1998); 5—Swiss Molasse basin (Burkhard and Sommaruga, 1998) modified from total subsidence using water:sediment density contrast); 6—Hoback Basin, Wyoming (Cross, 1986); 7—Green River Basin, Wyoming (Cross, 1986; Heller et al., 1986); 8—Magallanes Basin (Biddle et al., 1986).

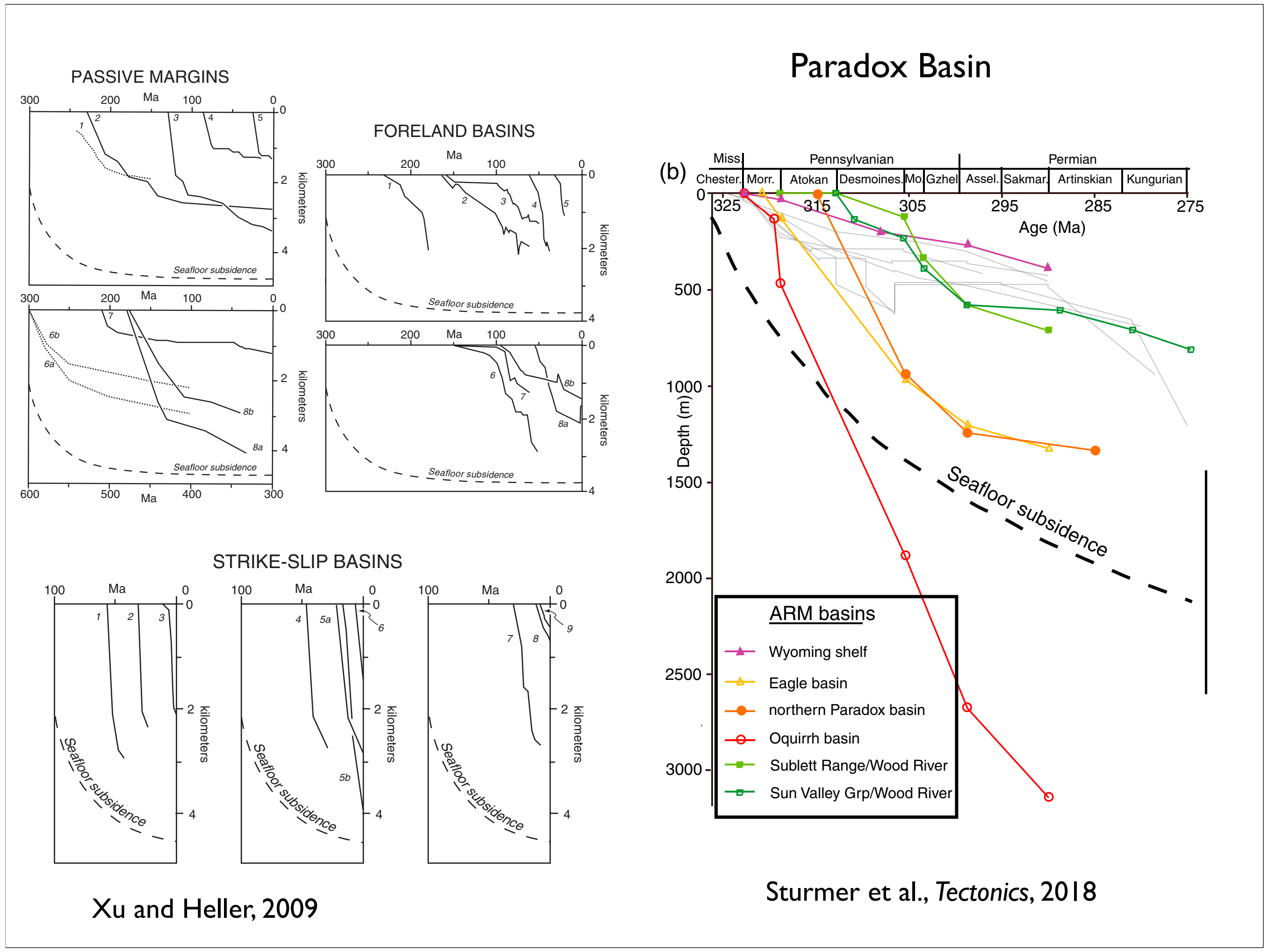

Figure 6. Tectonic subsidence of foreland basins. Locations shown in Figure 1. Thermal decay curve (dashed) for subsidence of cooling seafloor (Stein and Stein, 1992), minus 1500 m, is shown for comparison. 1—Eastern Avalonia, Anglo-Brabant fold belts (van Grootel et al., 1997); 2—Southern Alberta Basin (Gillespie and Heller, 1995); 3—San Rafael Swell, Utah (Heller et al., 1986); 4—Pyrenean foreland basin, Gombrèn (Vergés et al., 1998); 5—Swiss Molasse basin (Burkhard and Sommaruga, 1998) modified from total subsidence using water:sediment density contrast); 6—Hoback Basin, Wyoming (Cross, 1986); 7—Green River Basin, Wyoming (Cross, 1986; Heller et al., 1986); 8—Magallanes Basin (Biddle et al., 1986).

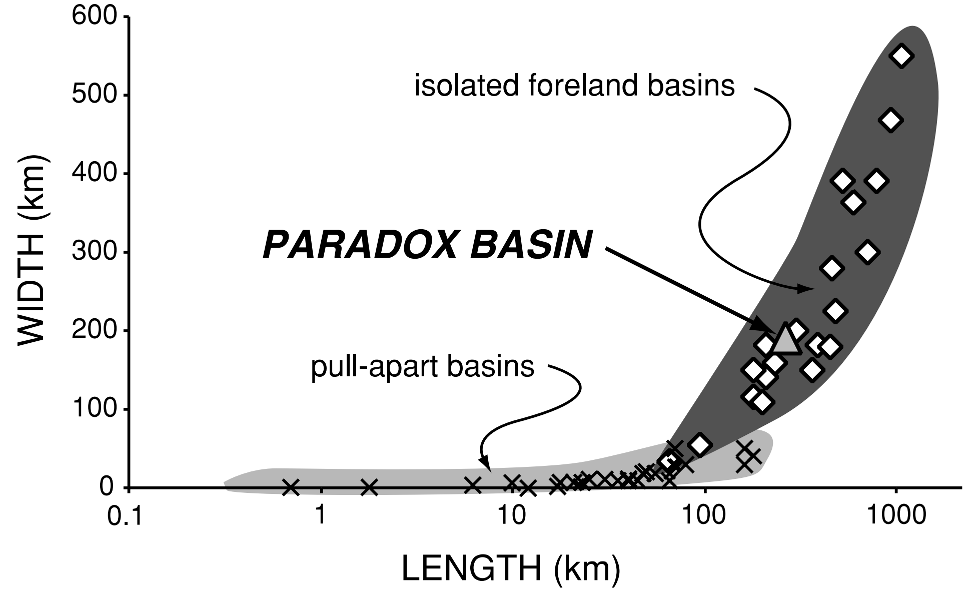

Barbeau, 2003

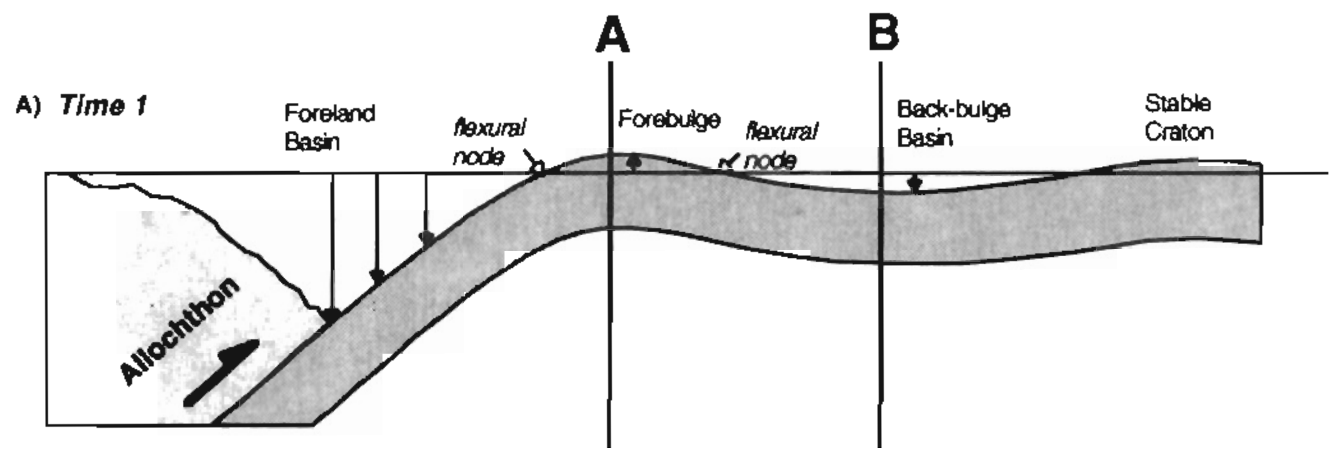
A
B
A) Time 1
Foreland
Basin
flexural
node
Forebulge
flexural
node
Back-bulge
Basin
Stable
Craton
Allochthon

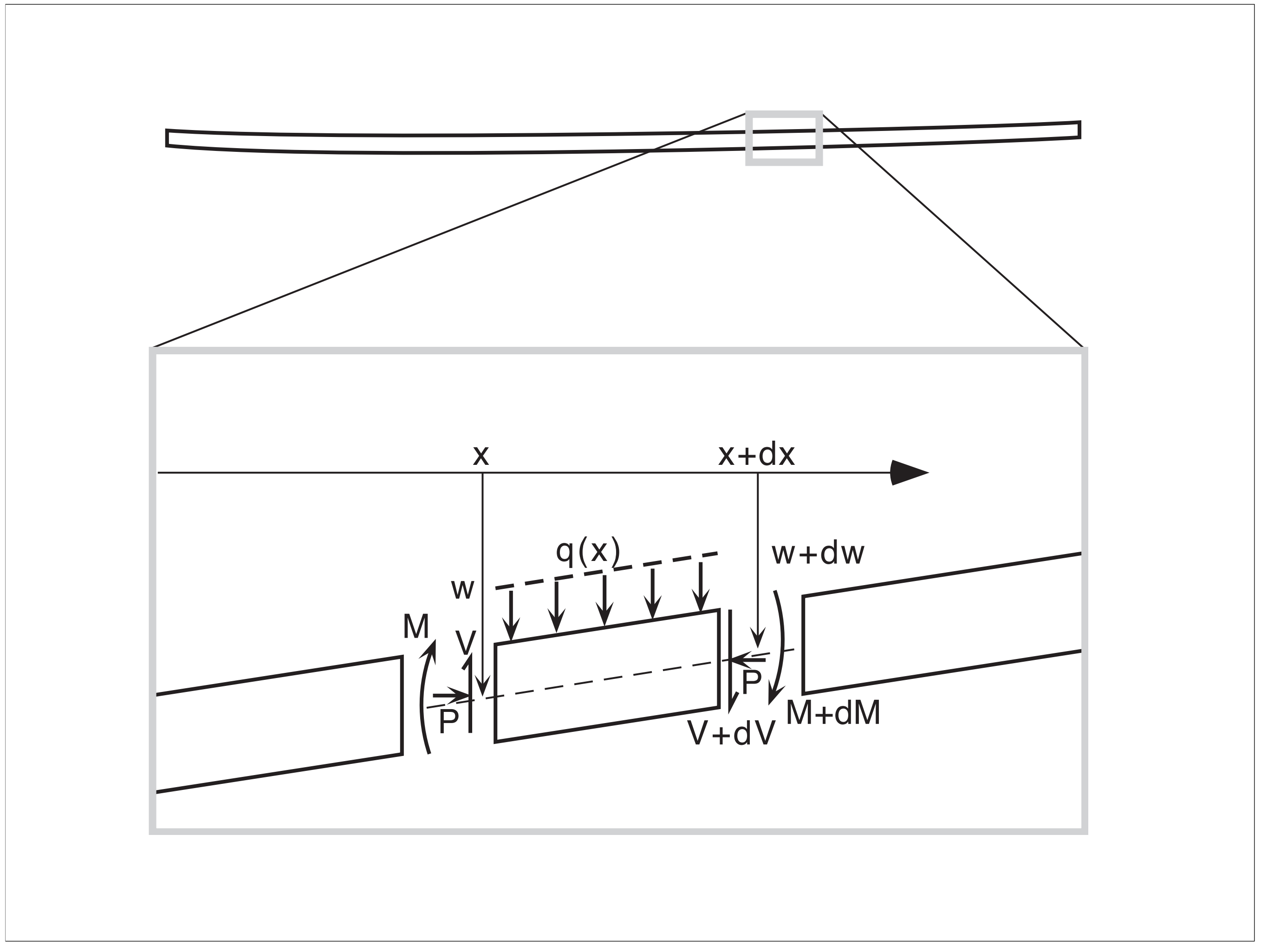
x
x+dx
q(x)
w
w+dw
M
V
P
P
M+dM
V+dV

$$q(x)\,dx + dV = 0$$

$$\frac{dV}{dx} = -q$$

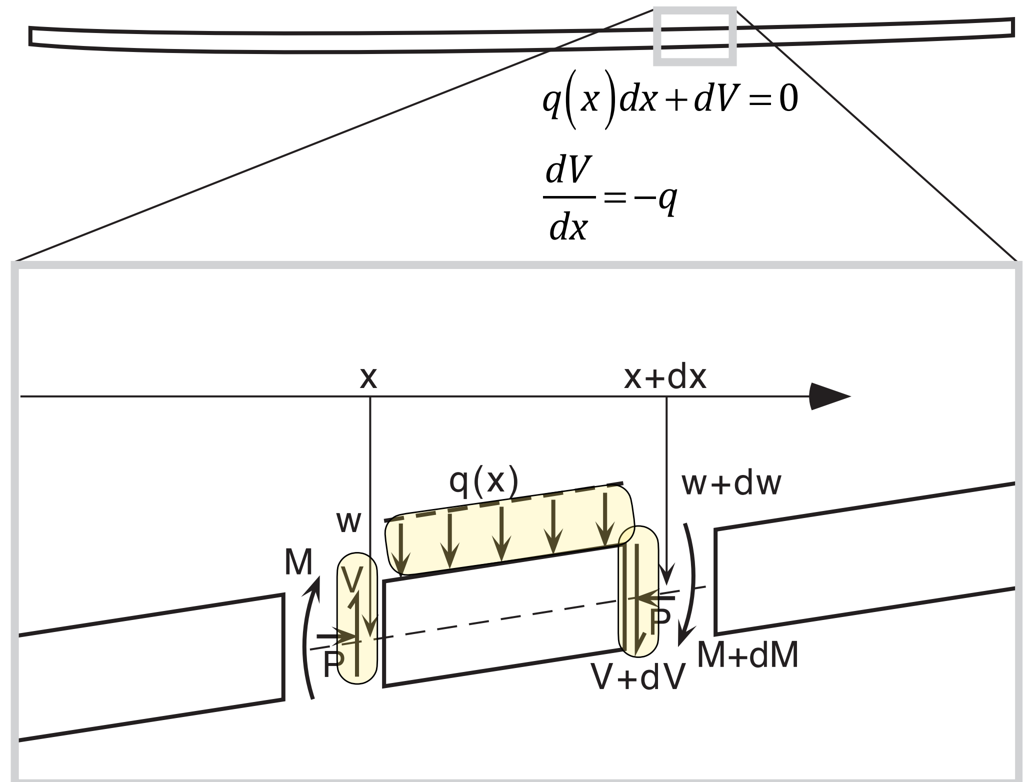

$$\frac{dV}{dx} = -q$$

$$dM - Pdw = Vdx$$

$$\frac{dM}{dx} = V + P\frac{dw}{dx}$$

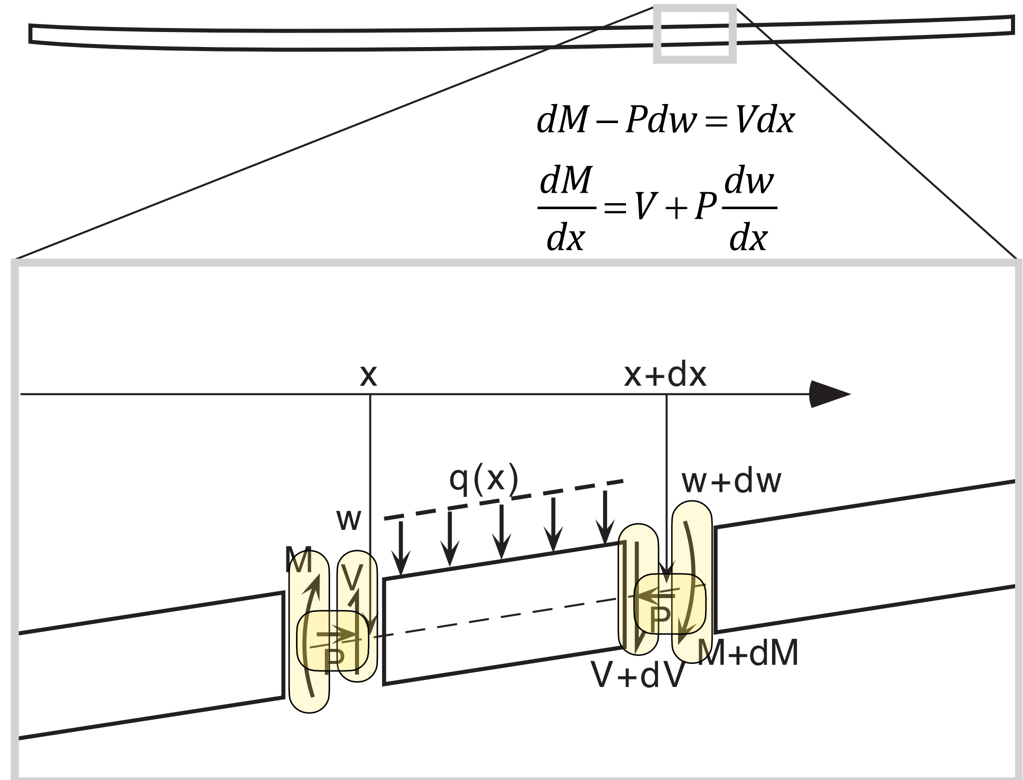

$$\frac{dV}{dx} = -q \qquad \frac{dM}{dx} = V + P\frac{dw}{dx} \qquad \frac{d^2M}{dx^2} = -q + P\frac{d^2w}{dx^2}$$

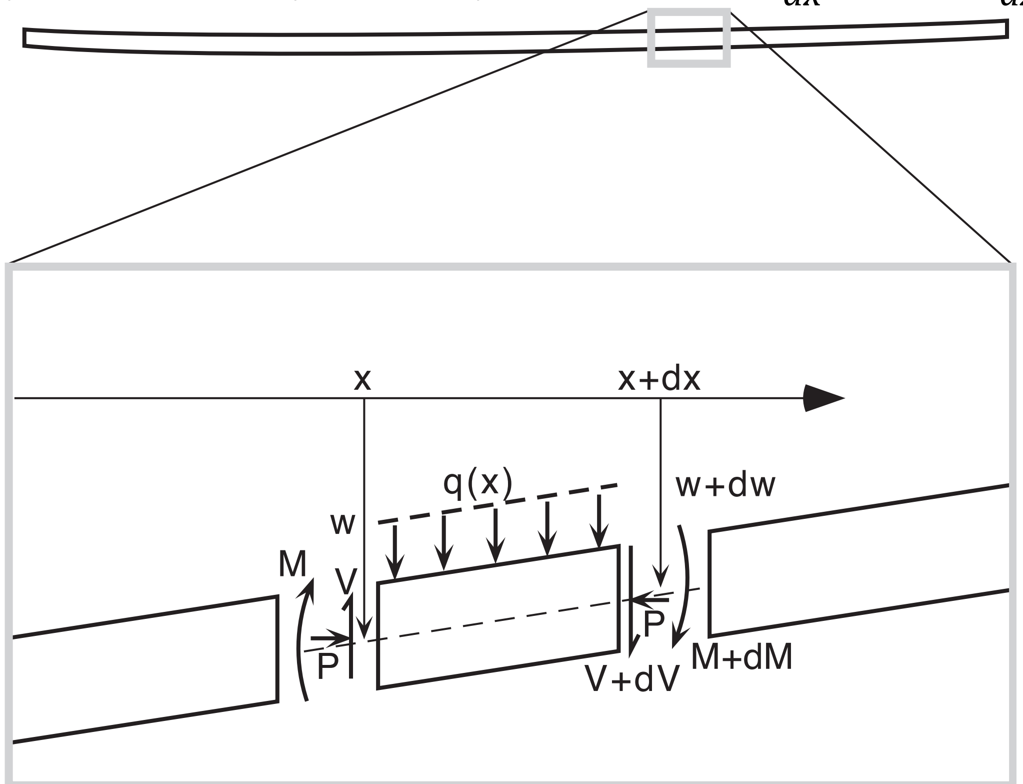

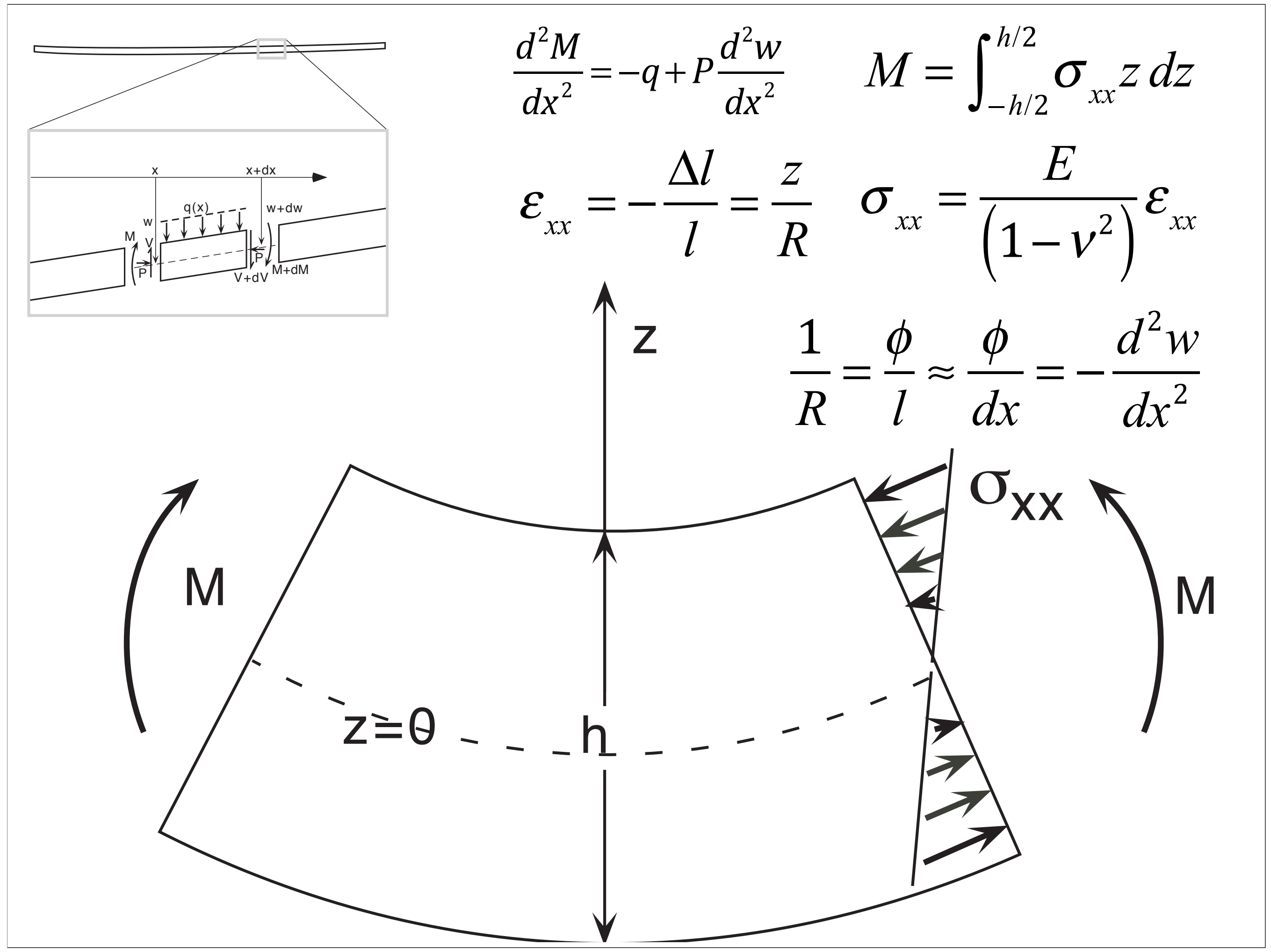

$\frac{d^2M}{dx^2} = -q + P\frac{d^2w}{dx^2}$
$M = \int_{-h/2}^{h/2} \sigma_{xx} z\, dz$
$\varepsilon_{xx} = -\frac{\Delta l}{l} = \frac{z}{R}$
$\sigma_{xx} = \frac{E}{(1-\nu^2)}\varepsilon_{xx}$
$\frac{1}{R} = \frac{\phi}{l} \approx \frac{\phi}{dx} = -\frac{d^2w}{dx^2}$
x
x+dx
q(x)
w
w+dw
M
P
V+dV
M+dM
z
σ_{xx}
M
M
z=0
h

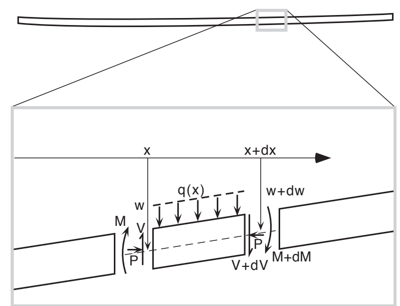

$$\frac{d^2M}{dx^2} = -q + P\frac{d^2w}{dx^2}$$

$$M = \int_{-h/2}^{h/2} \sigma_{xx} z \, dz$$

$$\varepsilon_{xx} = -\frac{\Delta l}{l} = \frac{z}{R}$$

$$\sigma_{xx} = \frac{E}{\left(1-\nu^2\right)}\varepsilon_{xx}$$

$$M = \frac{-E}{\left(1-\nu^2\right)}\frac{d^2w}{dx^2}\int_{-h/2}^{h/2} z^2 \, dz$$

$$= \frac{-E}{\left(1-\nu^2\right)}\frac{d^2w}{dx^2}\left(\frac{z^3}{3}\right)_{-h/2}^{h/2}$$

$$= \frac{-Eh^3}{12\left(1-\nu^2\right)}\frac{d^2w}{dx^2}$$

$$\frac{1}{R} = \frac{\phi}{l} \approx \frac{\phi}{dx} = -\frac{d^2w}{dx^2}$$

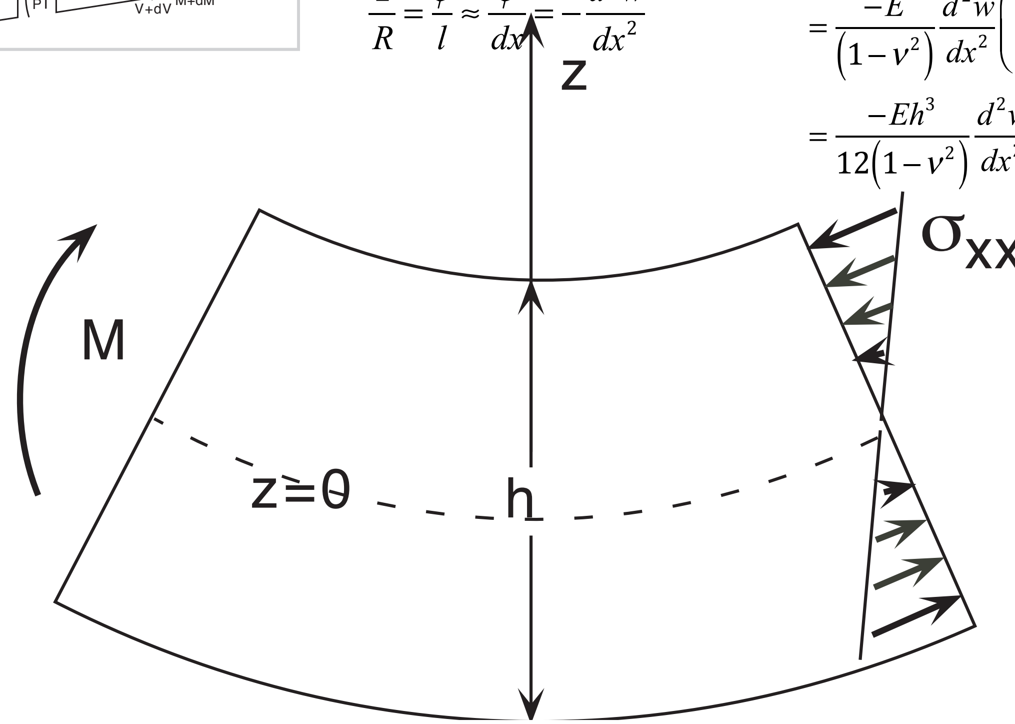

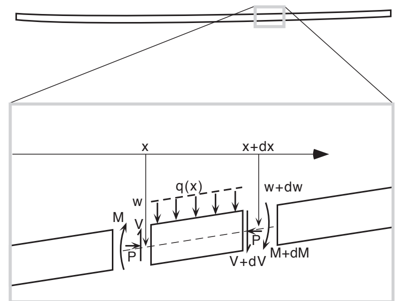

$$D\frac{d^4w}{dx^4} = q(x) - P\frac{d^2w}{dx^2}$$

$$D \equiv \frac{Eh^3}{12\left(1-\nu^2\right)}$$

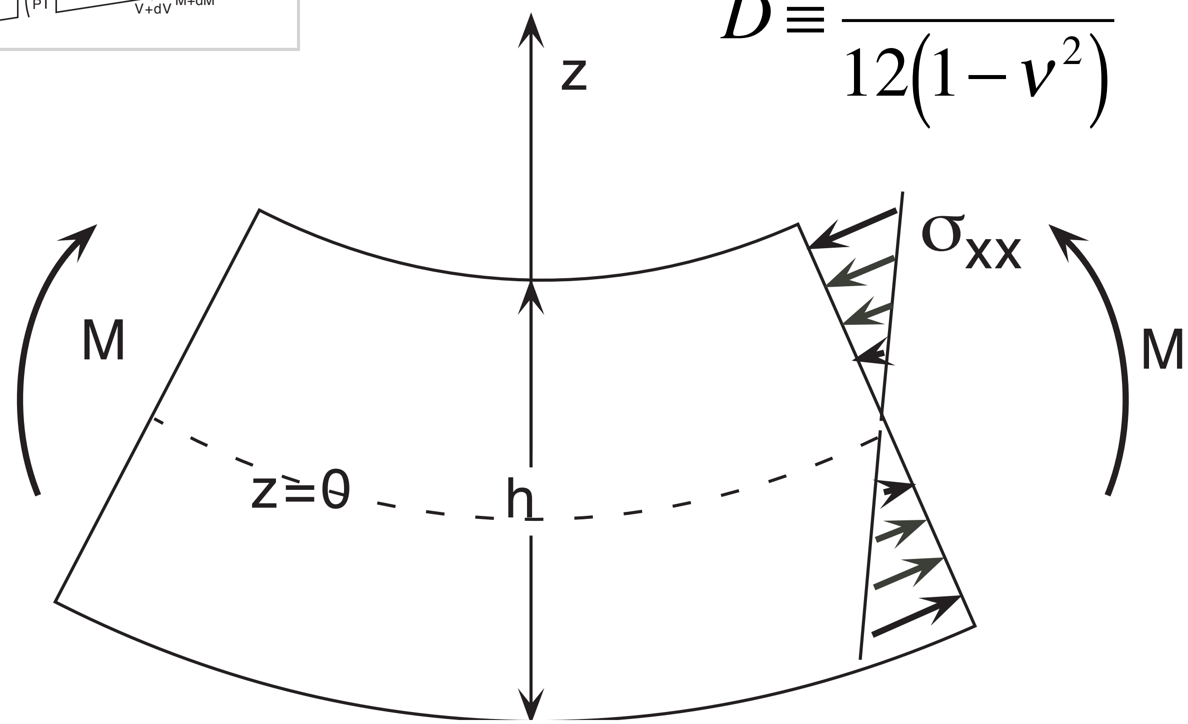

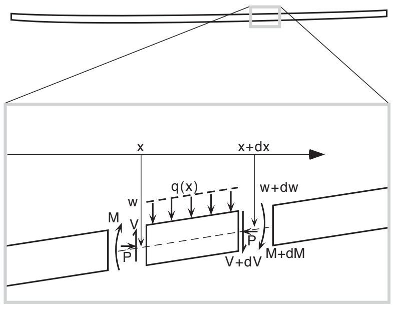

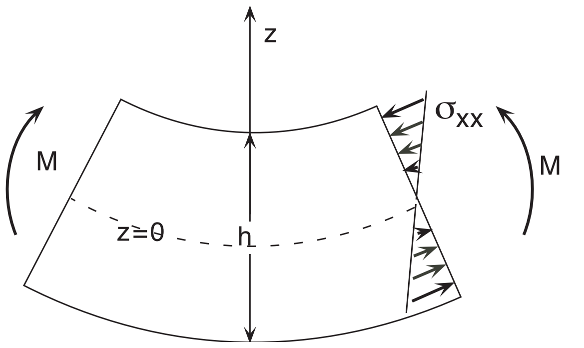

$$D\frac{d^4w}{dx^4}+P\frac{d^2w}{dx^2}+\left(\rho_a-\rho_f\right)gw=q_a(x)$$

$$q_a(x)=\rho_c g e_0 \sin 2\pi\frac{x}{\lambda}$$

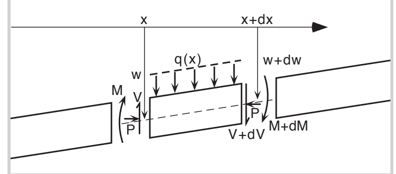

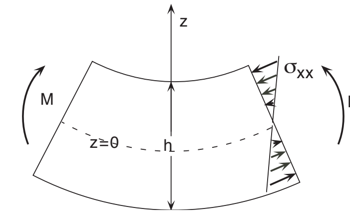

$$D\frac{d^4w}{dx^4}+P\frac{d^2w}{dx^2}+\left(\rho_a-\rho_f\right)gw=q_a(x)$$

$$q_a(x)=\rho_c g e_0 \sin 2\pi\frac{x}{\lambda}$$

$$w(x)=w_0 \sin 2\pi\frac{x}{\lambda}$$

$$w_0=\frac{e_0}{\dfrac{D}{g\rho_c}\left(\dfrac{2\pi}{\lambda}\right)^4+\dfrac{\rho_a}{\rho_c}-1}$$

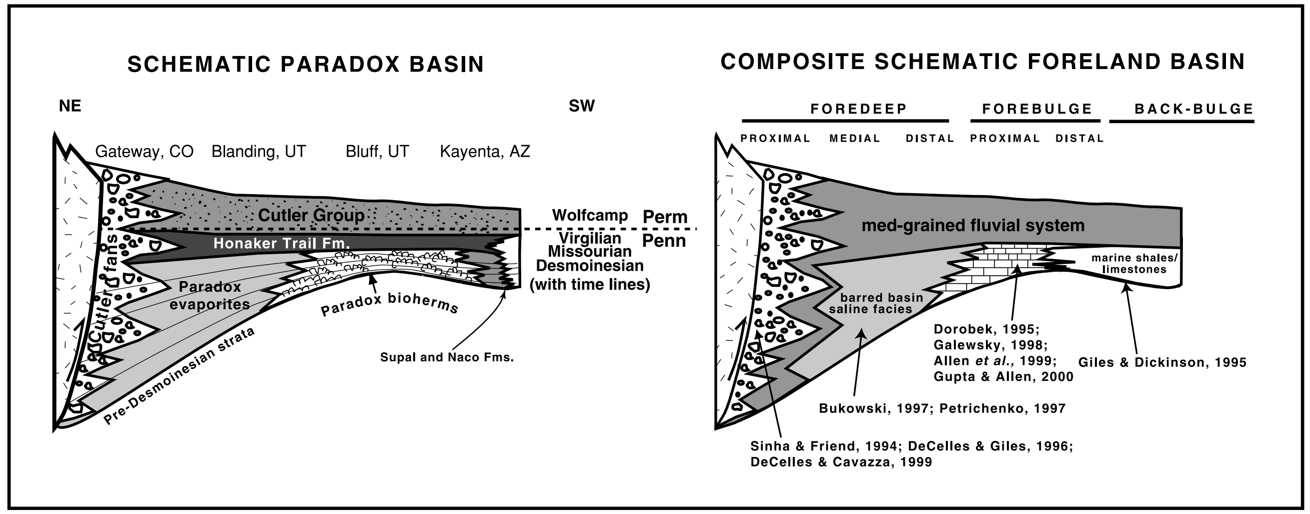

Fig. 7. (a) Schematic facies architecture of the Paradox Basin. (b) Schematic facies architecture of a composite restricted-marine isolated flexural basin. Facies recognized in other foreland basins are cited by reference.

Barbeau, 2003

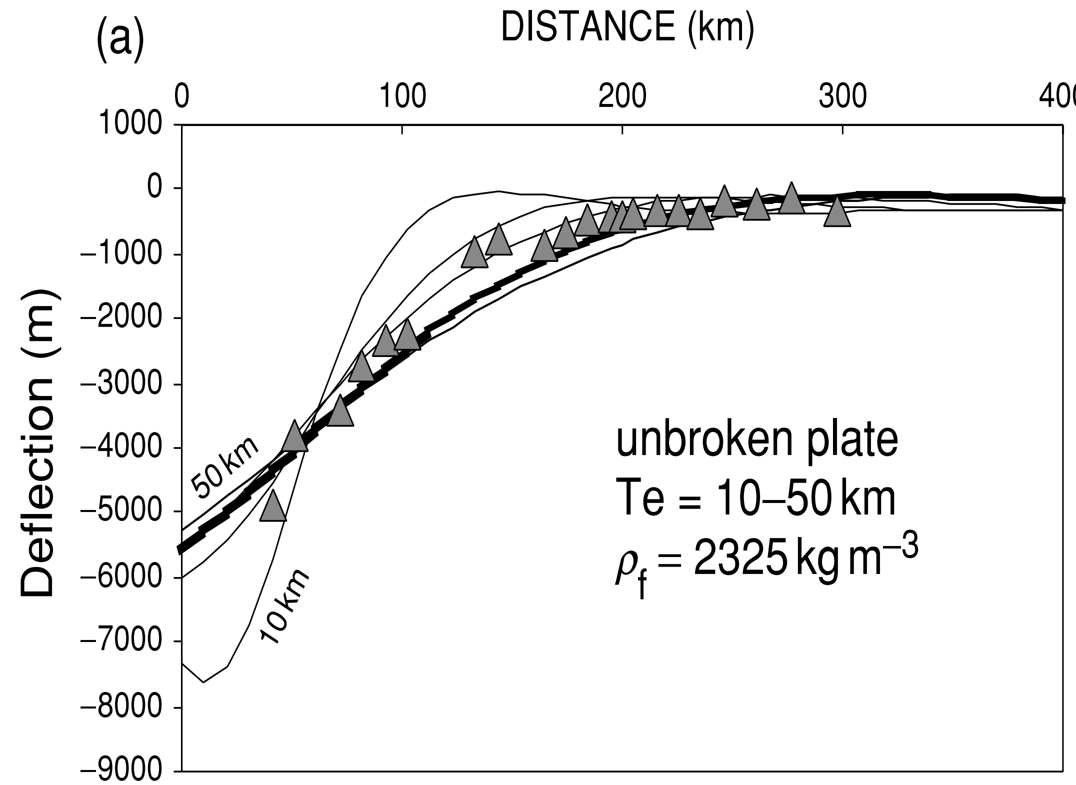

Barbeau, 2003

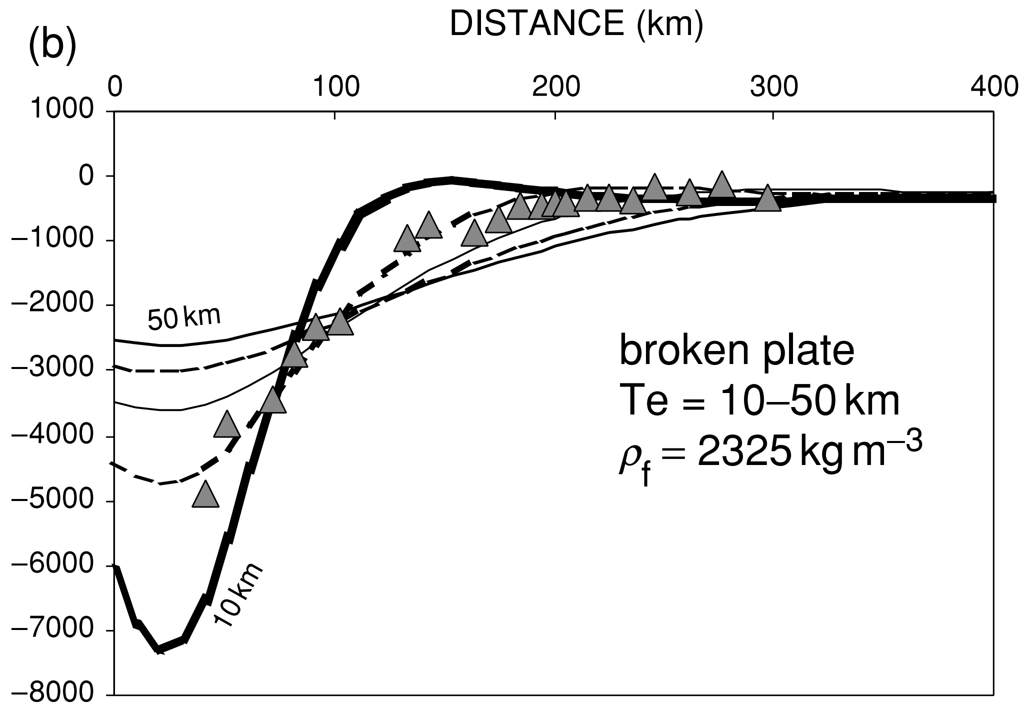

Barbeau, 2003

334-320 Ma Now again with faults...

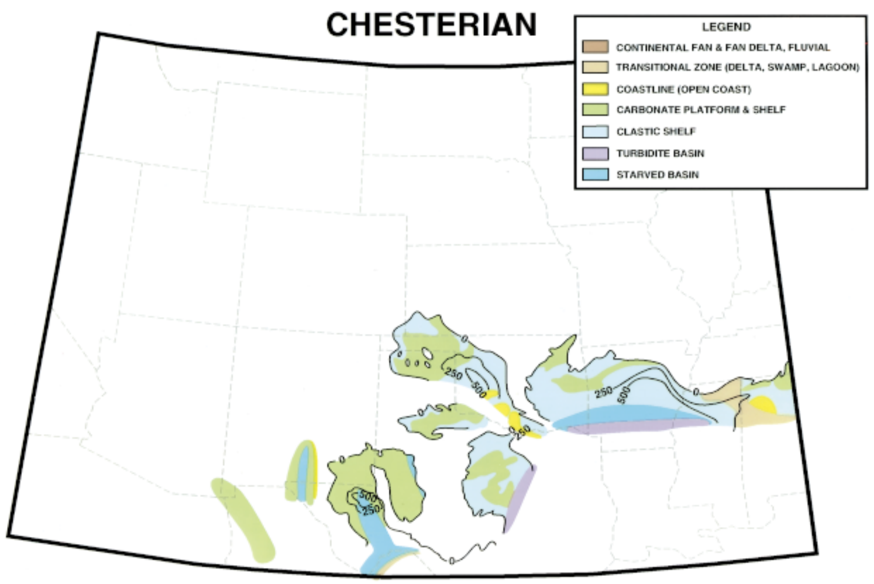

Ye et al., AAPG Bull, 1996

was 320-313, now 323-319 Ma

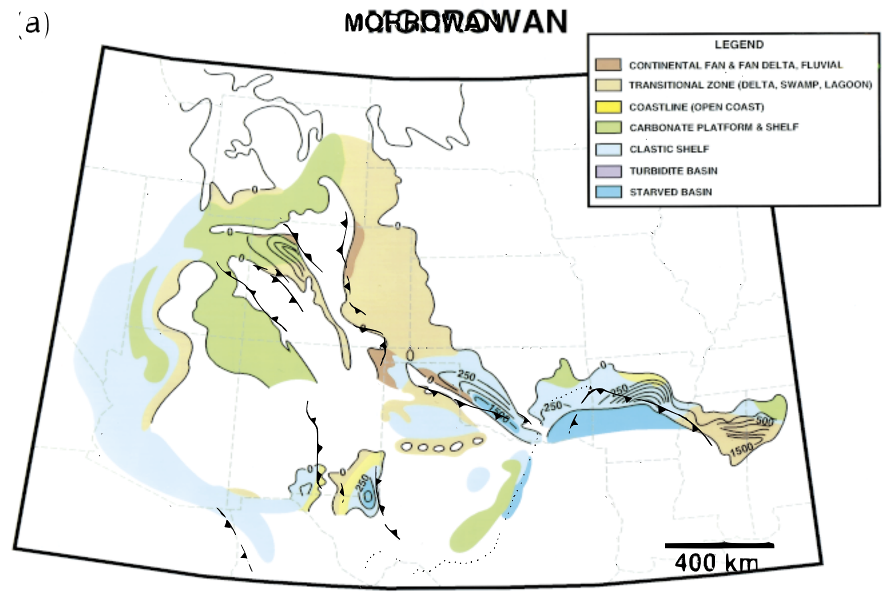

Ye et al., AAPG Bull, 1996

was 313-308 now 319-313 Ma

(b)

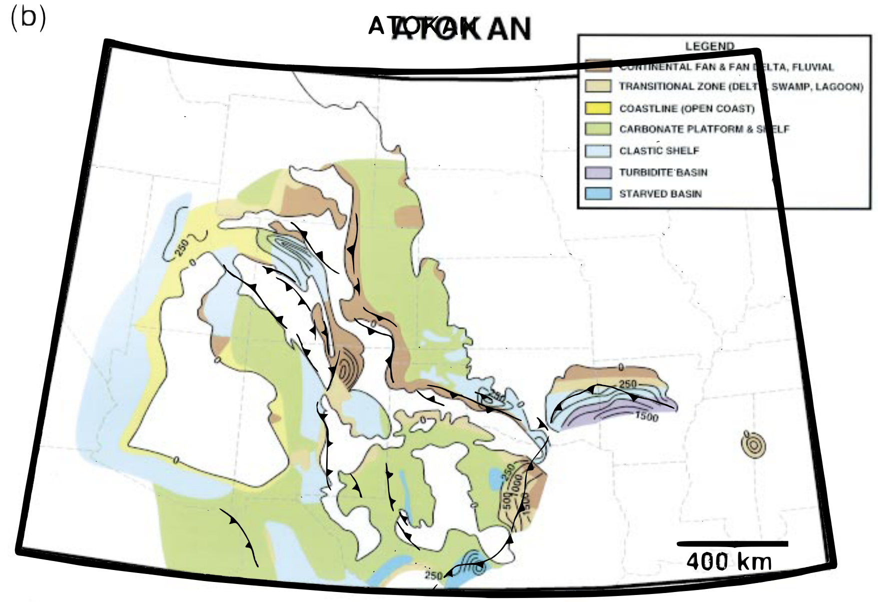

Ye et al., AAPG Bull, 1996

was 308-305 now 313-305.5 Ma

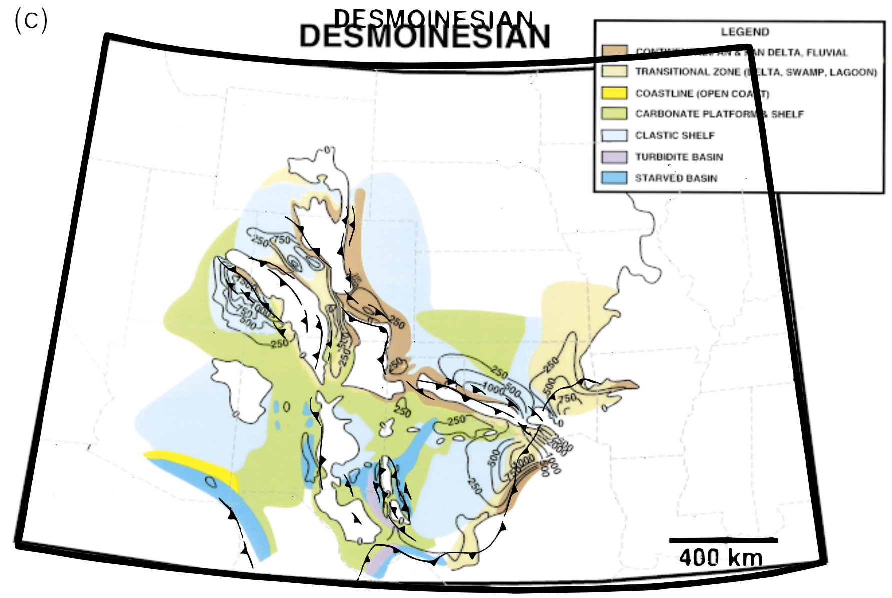

Ye et al., AAPG Bull, 1996

was 305-303 now 305.5-303.2 Ma

(d)

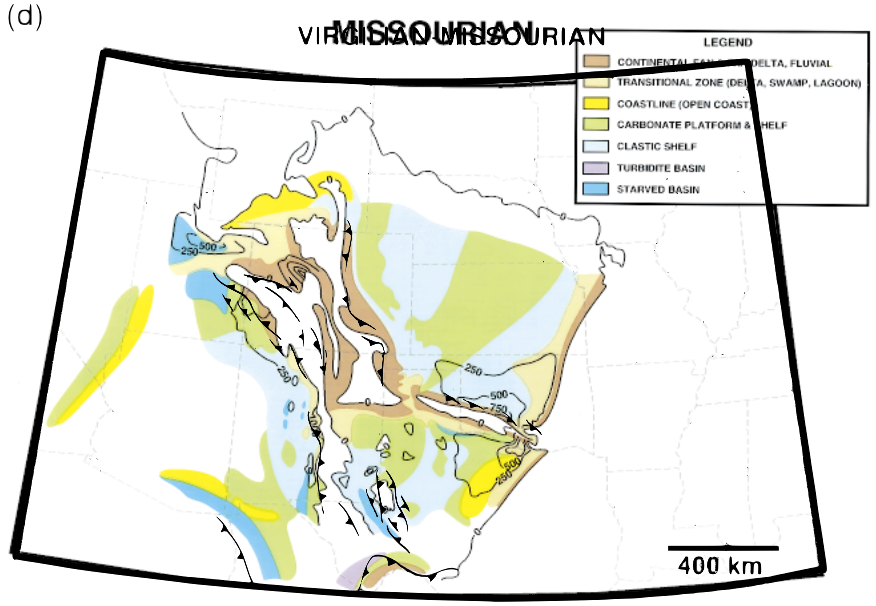

Ye et al., AAPG Bull, 1996

303-296 now 303.2-300 Ma

(d)

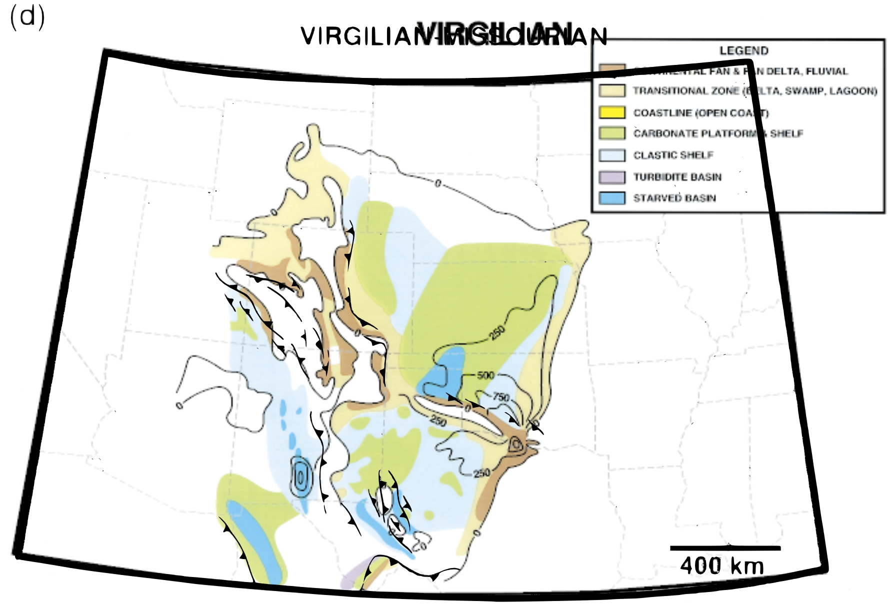

Ye et al., AAPG Bull, 1996

was 296-280 now 300-~280 Ma (Permian)

(e)

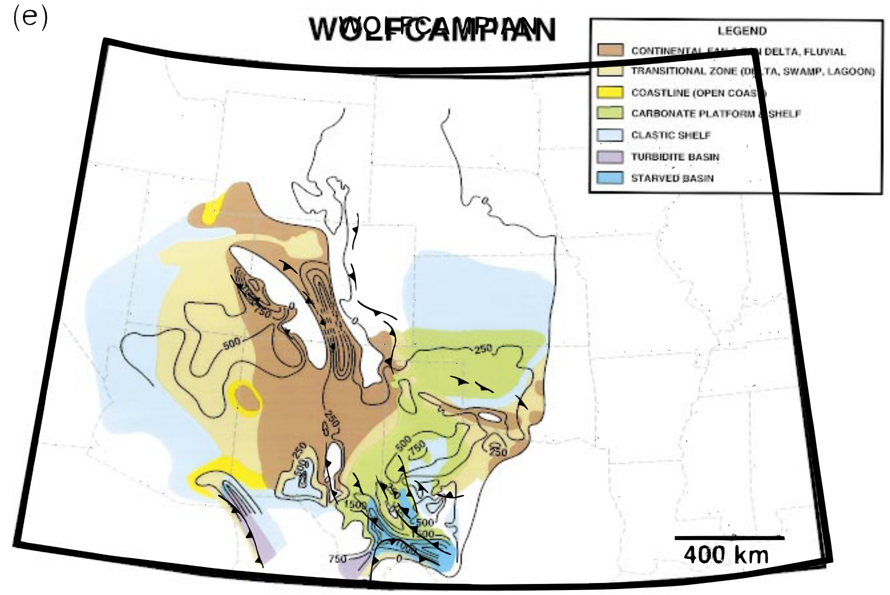

Ye et al., AAPG Bull, 1996

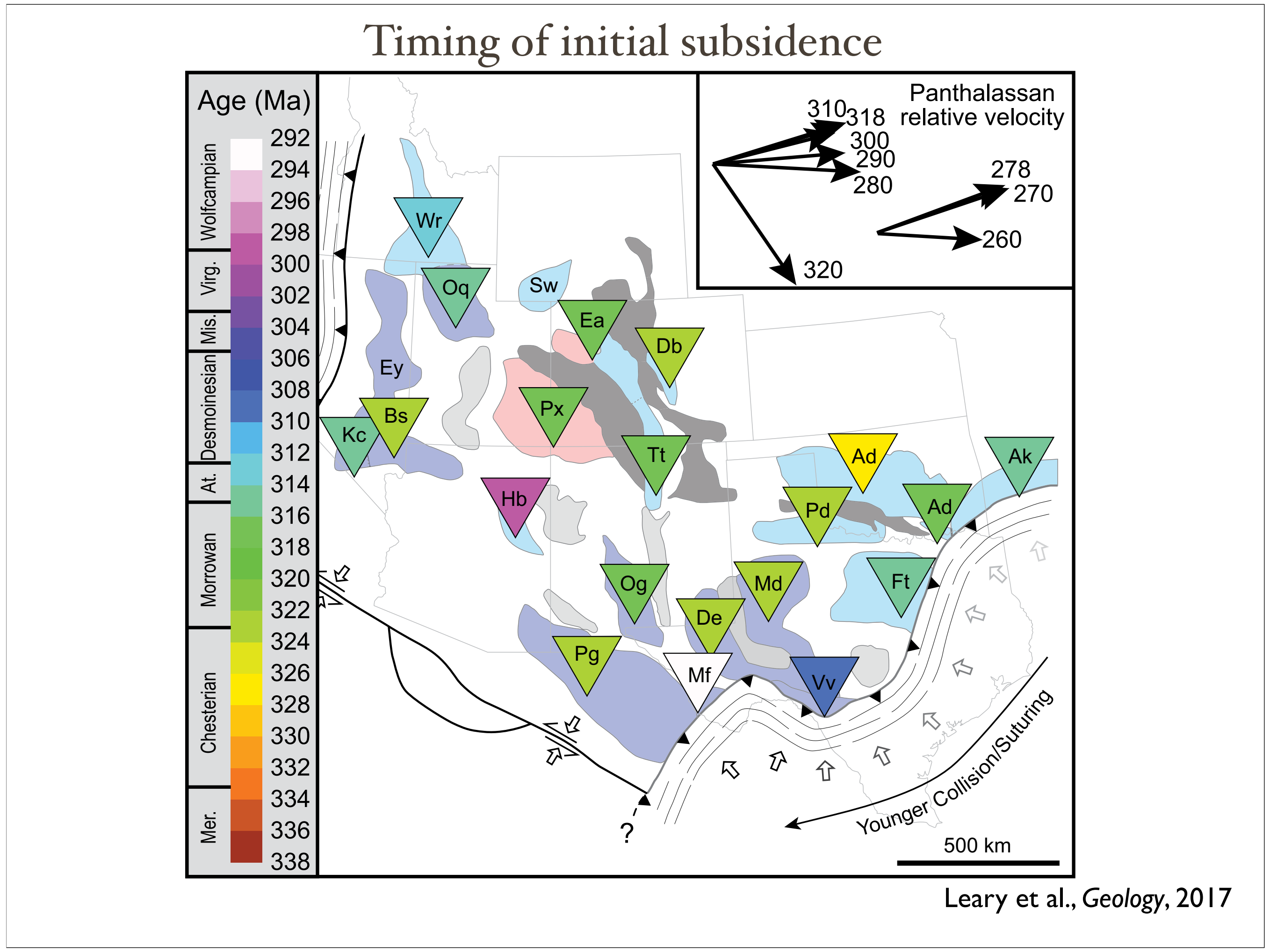

Argue all the ARM basins originated in early Morrowan.

Basins: Ha—Havallah; Wr—Wood River; Ey—Ely; Bs—Bird Springs; Kc—Keeler Canyon; Oq—Oquirrh; Sw—Sweetwater Trough; Ea—Eagle; Px—Paradox; Hb—Holbrook; Tt—Taos Trough; Og—Orogrande; Db—Denver; Pg—Pedregosa; Mf—Marfa; De—Delaware; Vv—Val Verde; Md—Midland; Pd—Palo Duro; Ad—Anadarko; Ft—Fort Worth; Ad—Ardmore; Ak—Arkoma; Bw—Black Warrior. Uplifts: Fr—Front Range; Uu—Uncompahgre; Pi—Piute; Zd—Zuni-Defiance; Pd—Pedernal; Fl—Florida; Cb—Central Basin Platform; Lu—Llano; Wu—Wichita. CAB—Caborca block.

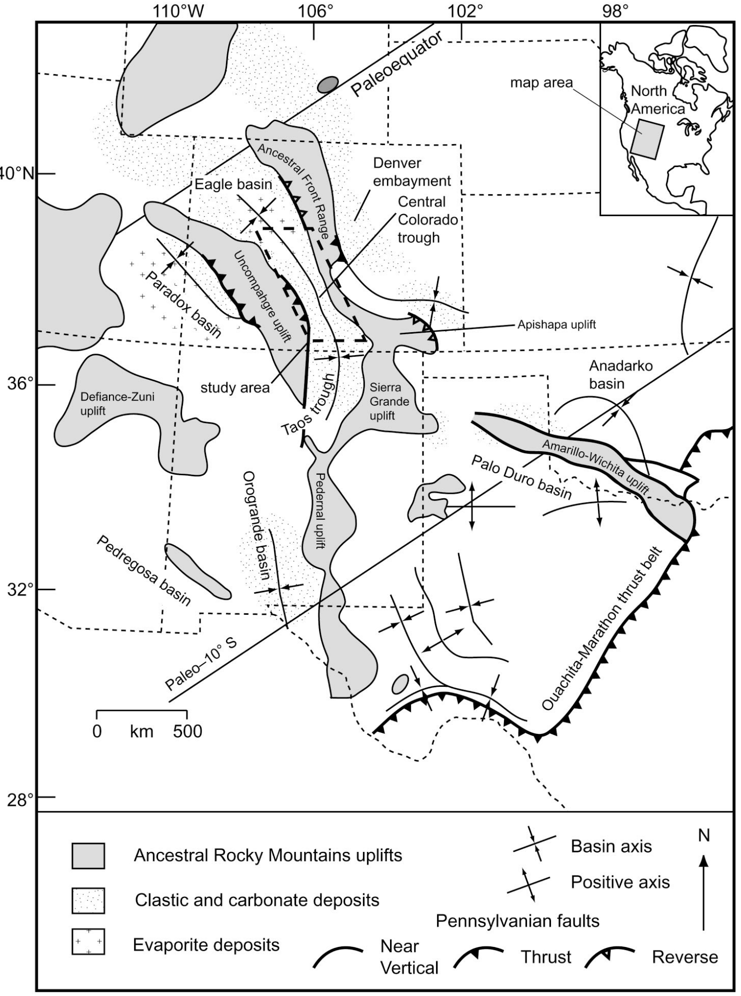

Hoy and Ridgway 2002

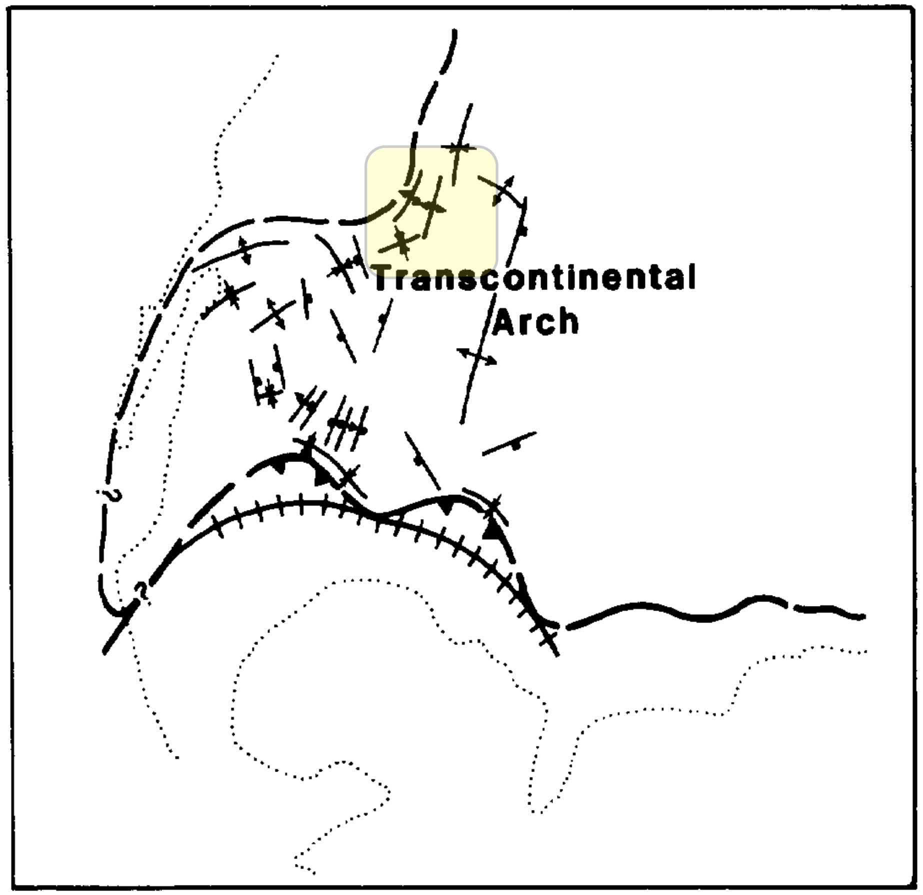

Kluth, AAPG Mem 41, 1986

Kluth and Coney (and many others) have noted the temporal and spatial association of Ancestral Rockies with Ouachita

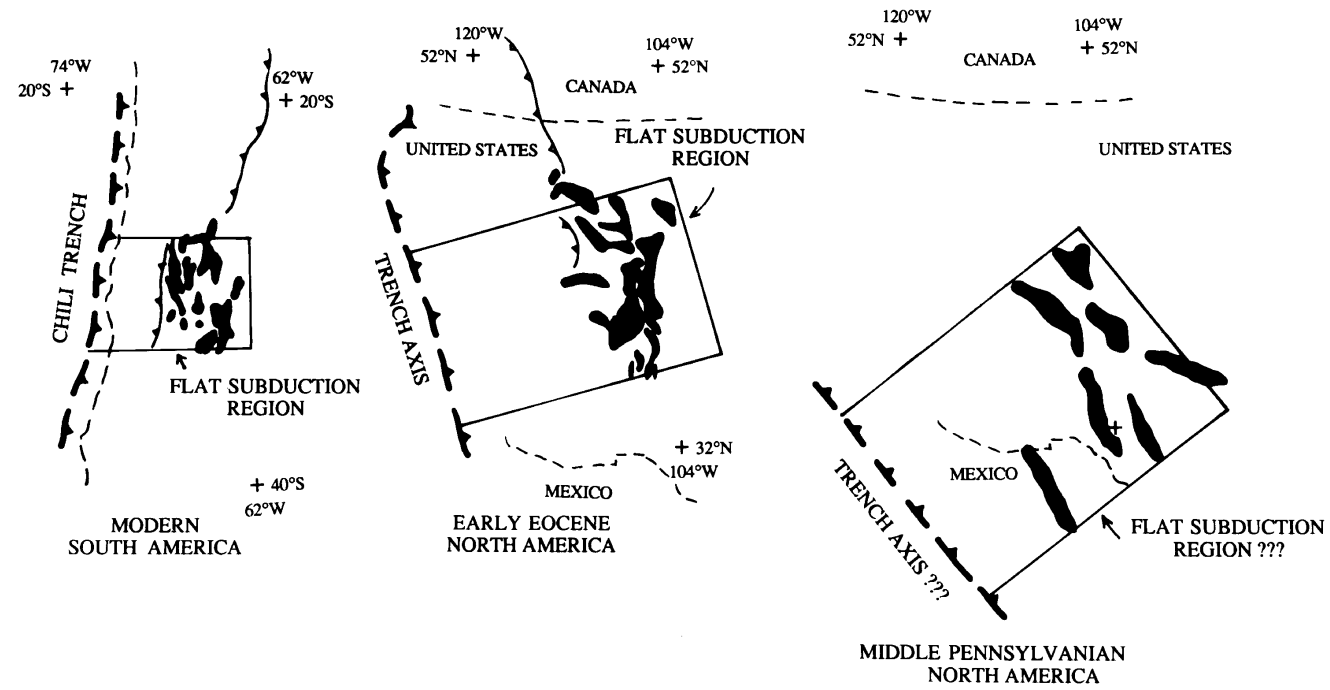

Ye et al., AAPG Bull, 1996

To date, still no evidence of Pennsylvanian arc.

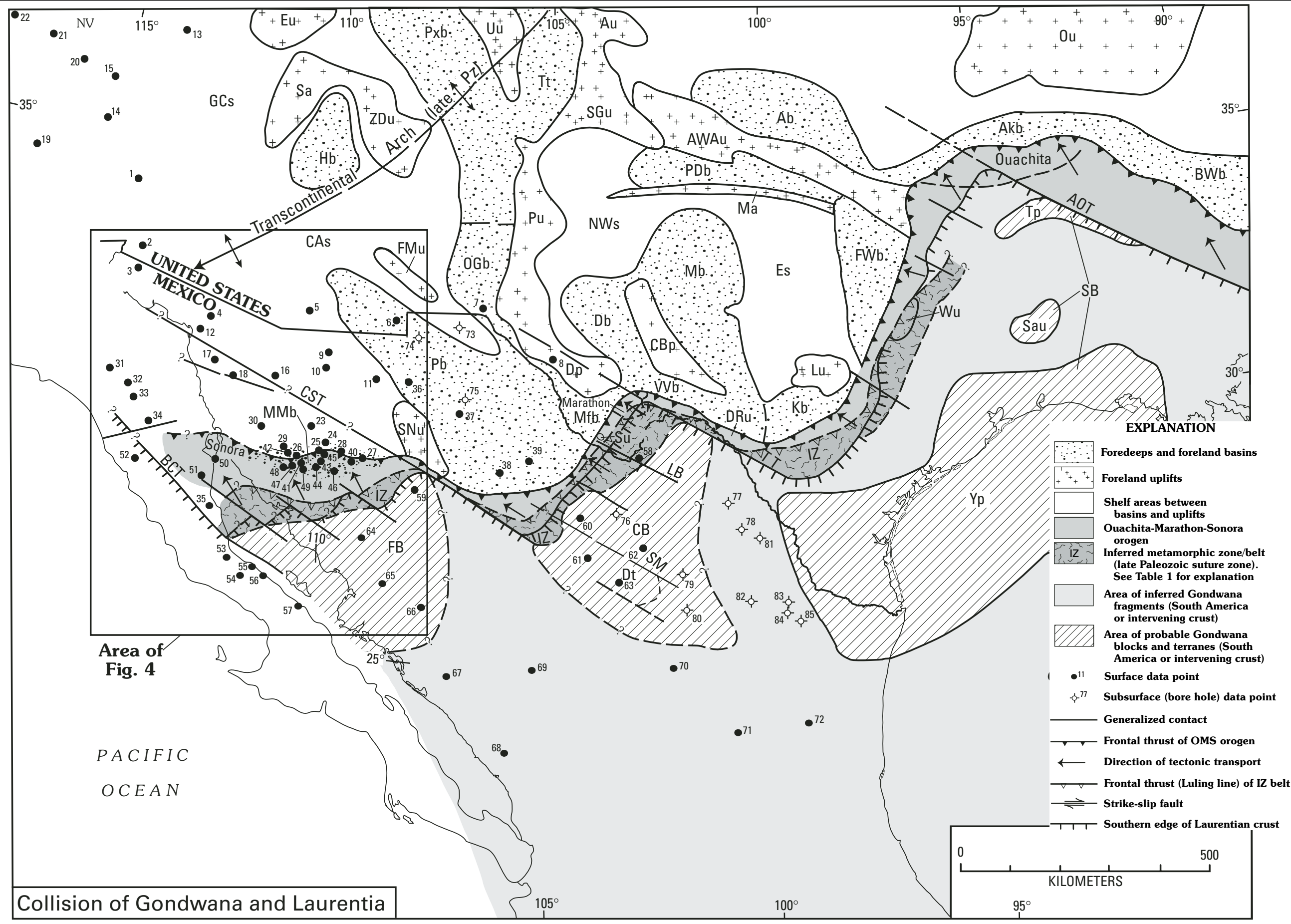

Figure 3. Regional map of southern Laurentia showing late Paleozoic geologic features and localities mentioned in text and described in Table 1, and location of Figure 4.

Poole et al., GSA SP 393, 2005

Notice that the transport directions inferred are to the NW (right-lateral ss). Paradox Basin (Pxb) and Uncompahgre uplift (Uu) at top.

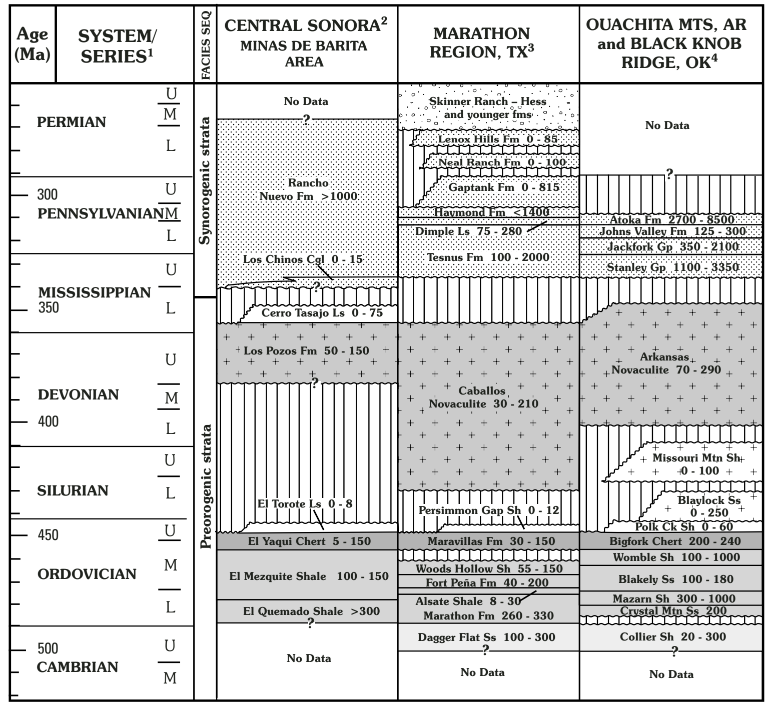

[1]**System/Series boundaries:** Claoué-Long et al. (1992), Cooper (1999), Harland et al. (1990), Jin et al. (1997), Landing et al. (2000), Menning et al. (2000), Sandberg and Ziegler (1996), Sando (1985), Stone et al. (2000), Tucker et al. (1998).
[2]**Sonora:** Poole et al. (in progress).
[3]**Marathon:** Barrick and Noble (1995), Ellison and Powell (1989), Ethington et al. (1989), Finney (1986), McBride (1989), Noble (1990, 1994), Ross (1978, 1979, 1986), Ross and Ross (1995).
[4]**Ouachita:** Barrick and Haywa-Branch (1994), Ethington et al. (1989), Finney (1986), Hass (1951), Lowe (1989), Morris (1989).

Figure 5. Generalized stratigraphic sections characteristic of the Sonora, Marathon, and Ouachita segments of the Ouachita-Marathon-Sonora orogenic system. Thickness ranges in meters. Similar patterns represent correlative strata.

Poole et al., GSA SP 393, 2005

Notes similarities to connect to region to east.

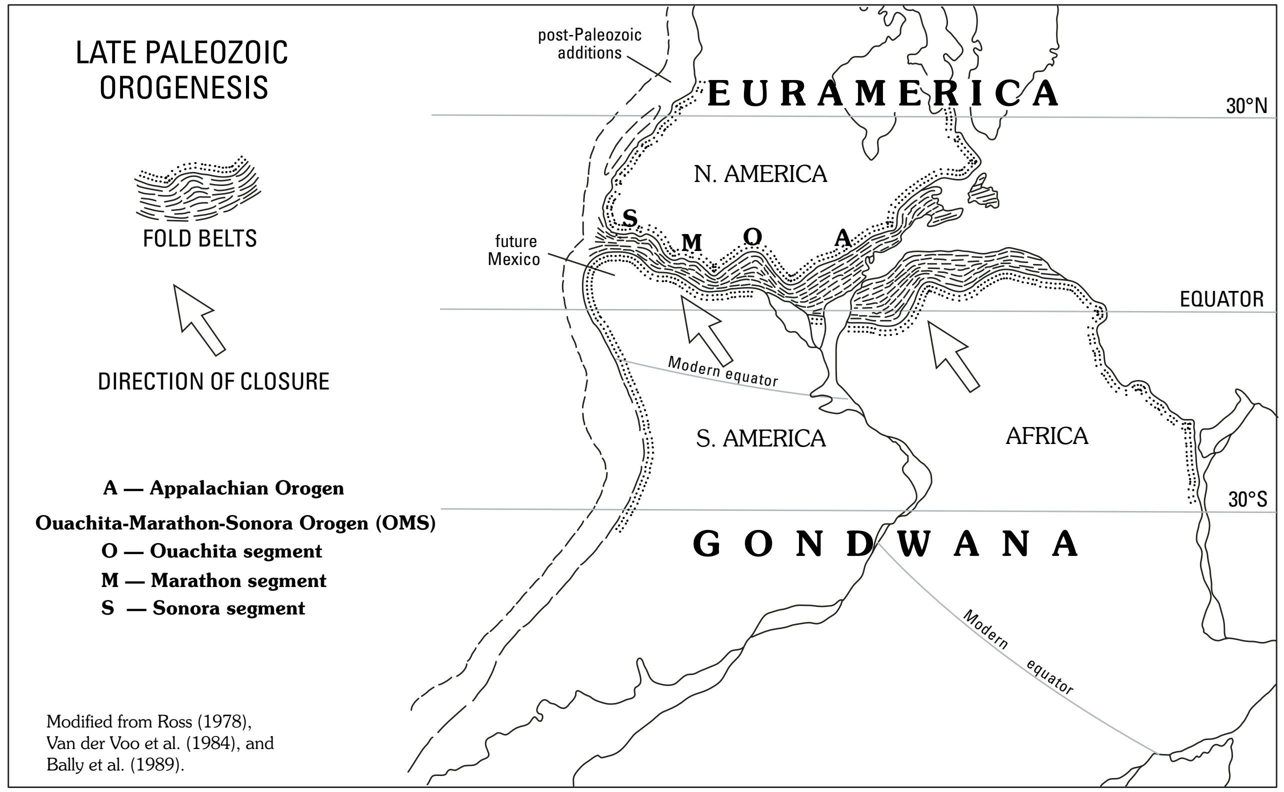

Poole et al., GSA SP 393, 2005

Note that this would make Sonoran margin right-lateral.

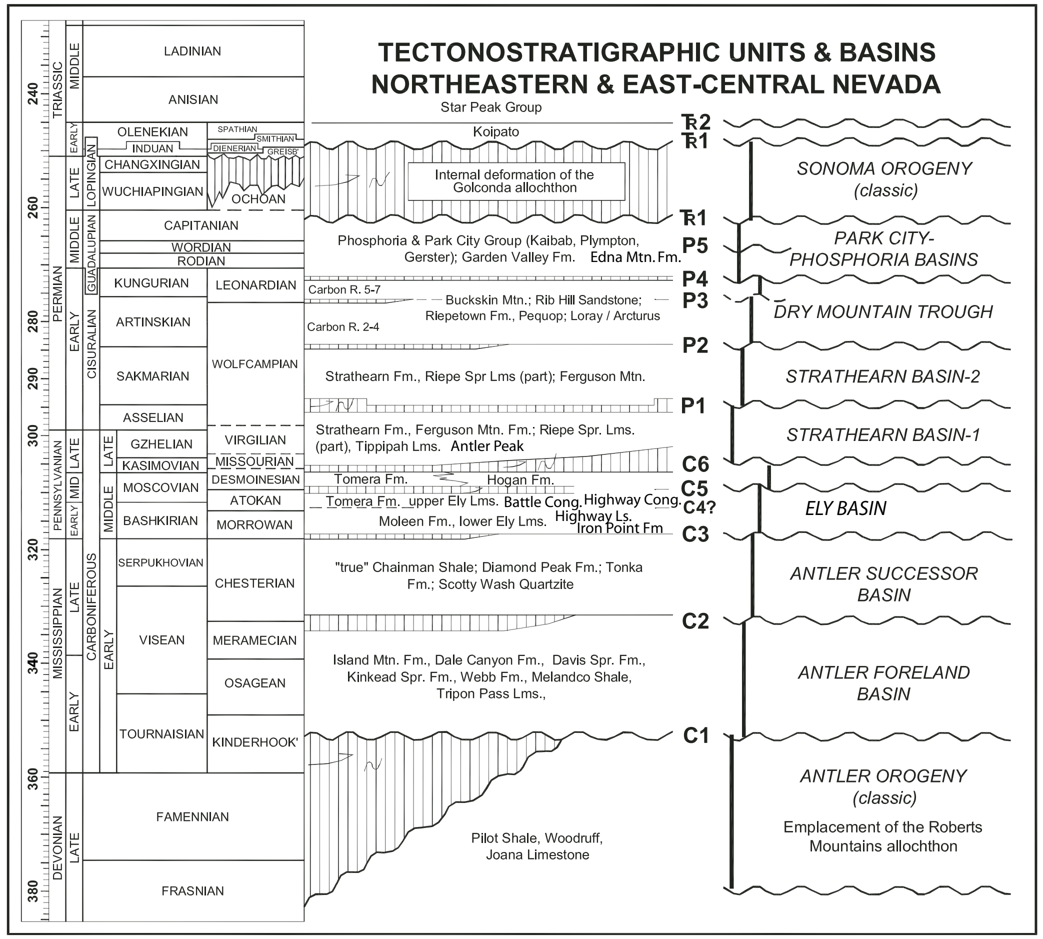

Cashman et al, GSA Flied Guide 11, 2008

Western margin had been characterized as lacking deformation in Pennsylvanian, which has lately been challenged.

Carlin Canyon, central Nevada

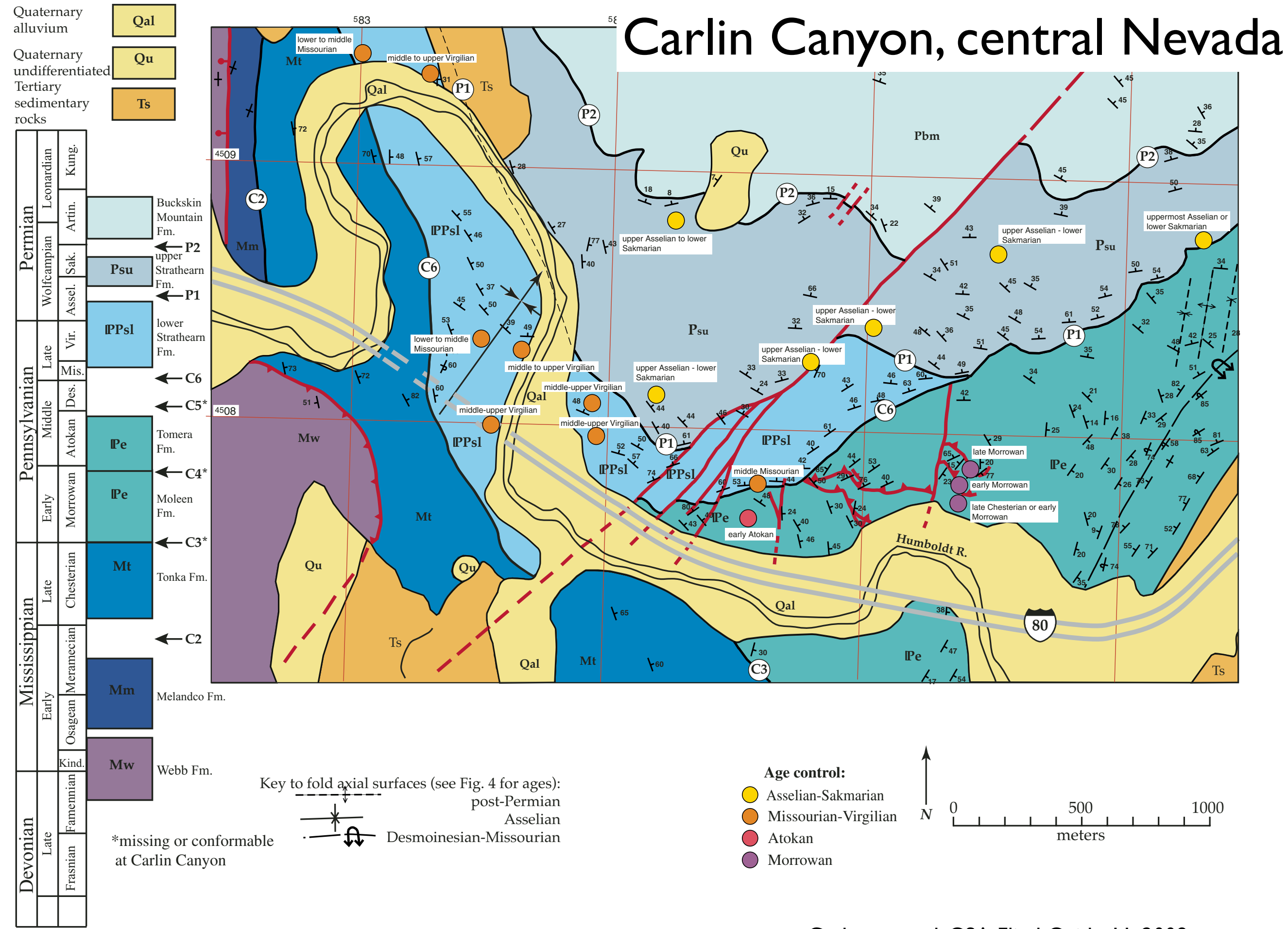

Cashman et al, GSA Flied Guide 11, 2008

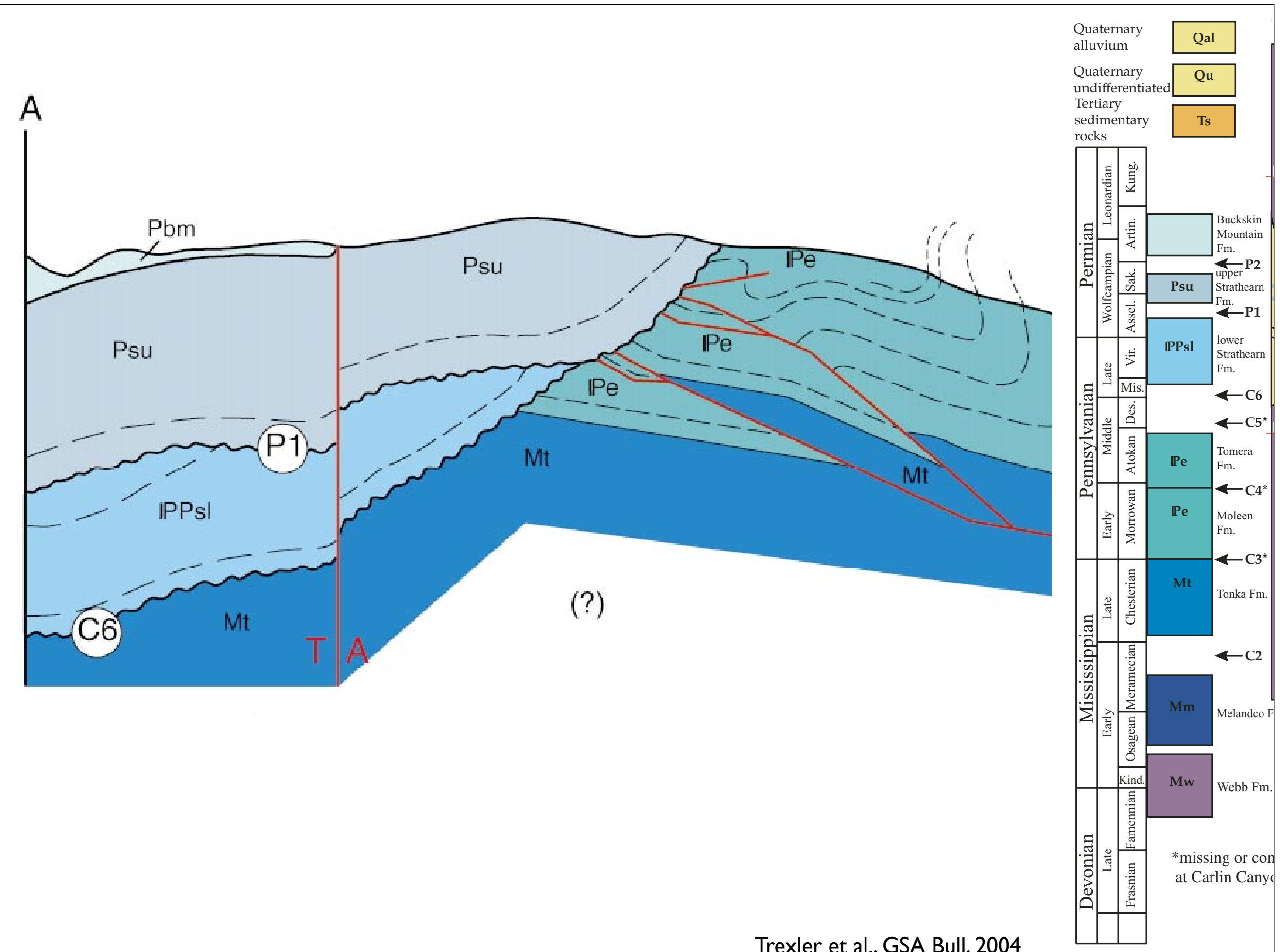

Trexler et al., GSA Bull, 2004

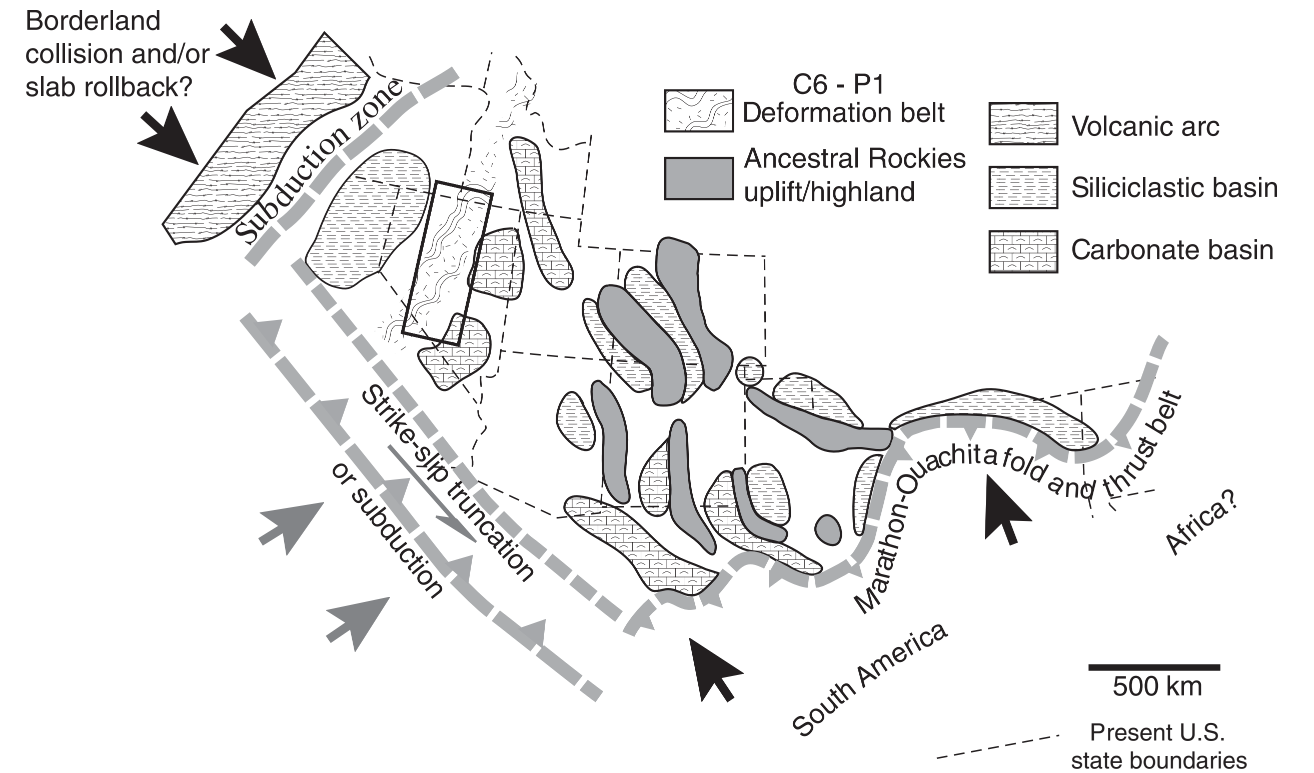

Cashman et al., GSA Bull, 2010

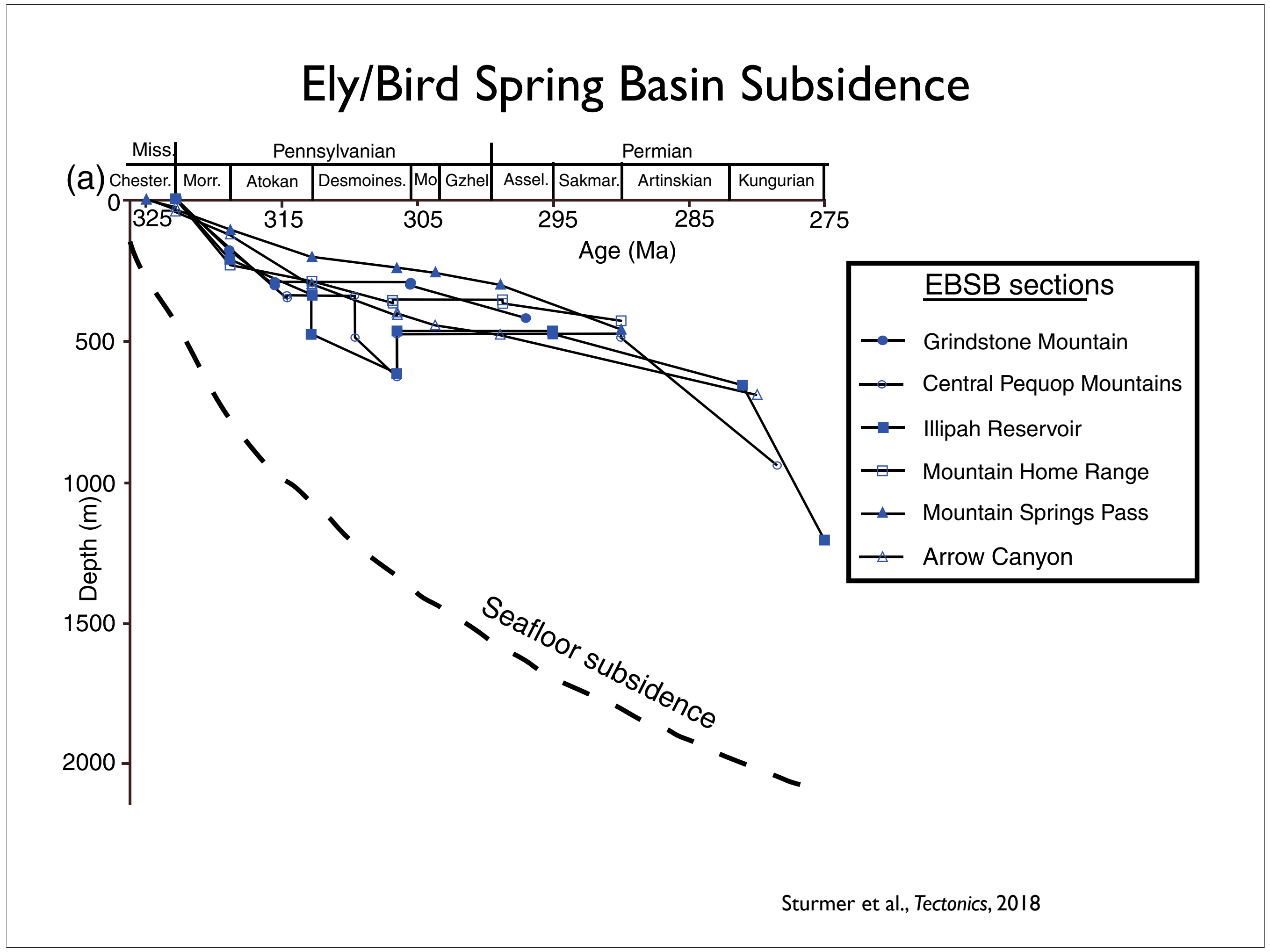

Note convex-up patterns—argue this is from migrating thrust loads.

Ely/Bird Spring Basin Subsidence

ARM Basins Subsidence

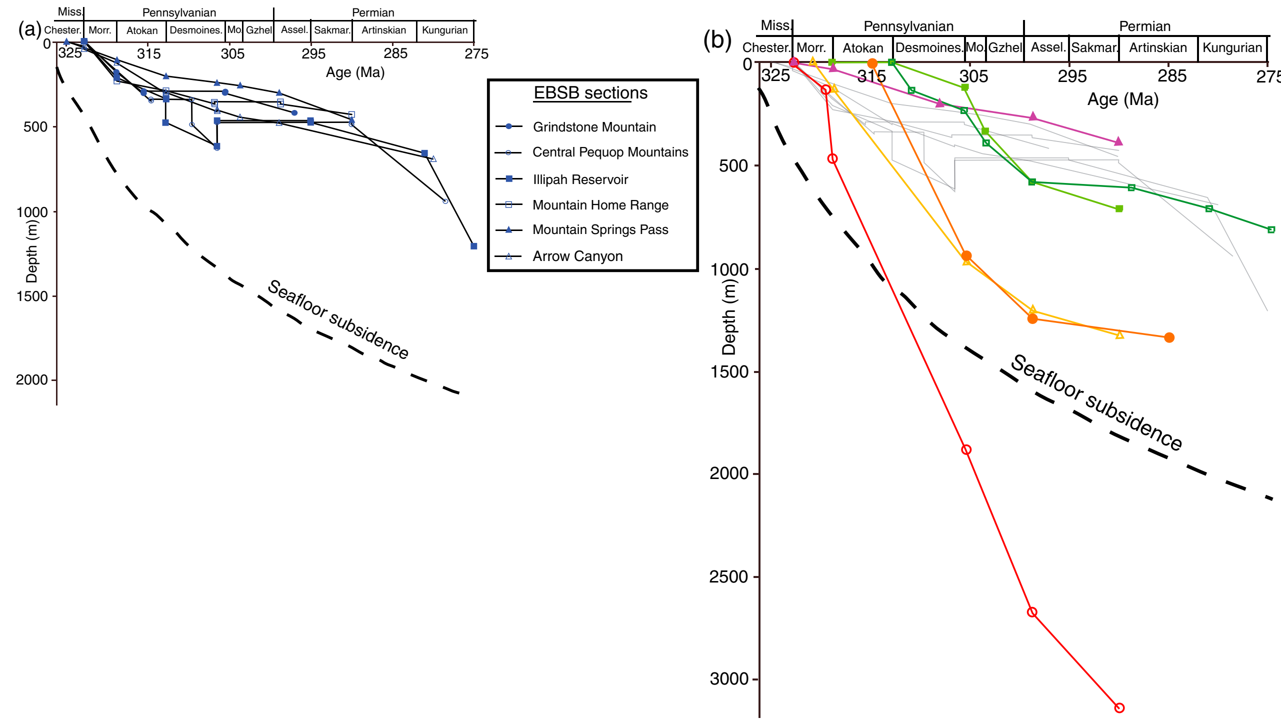

Sturmer et al., *Tectonics*, 2018

As opposed to classic Ancestral Rockies uplifts where loads were stationary.

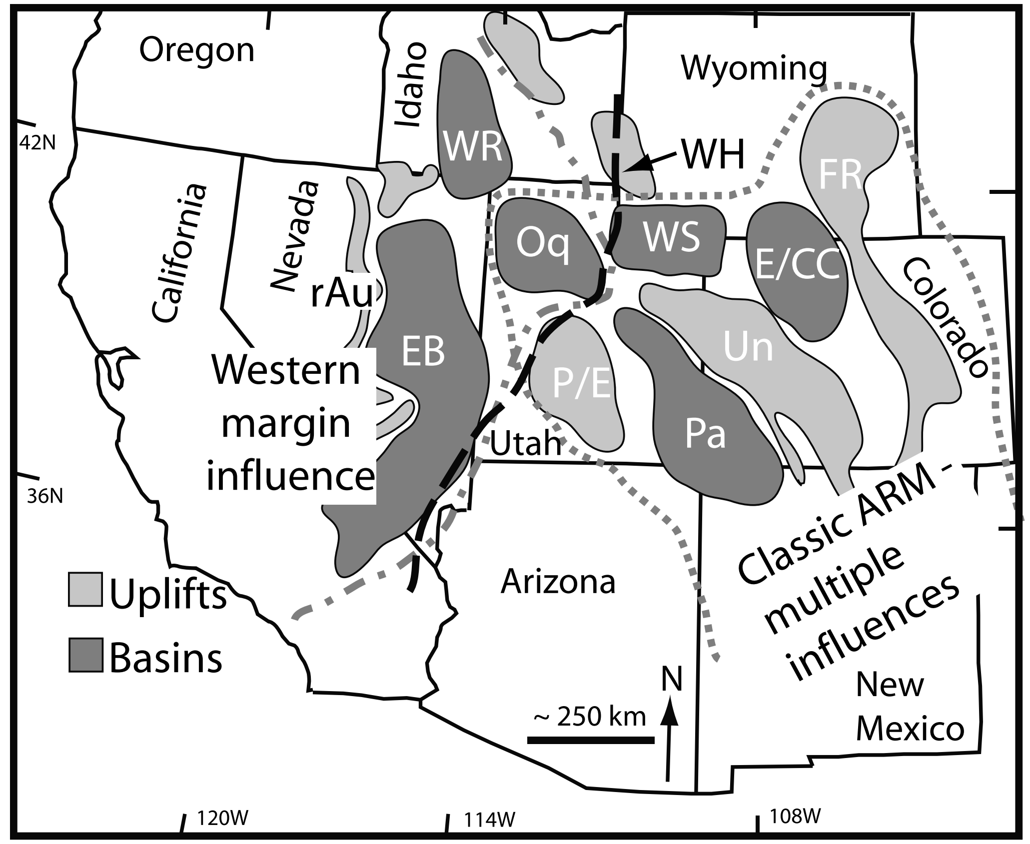

Sturmer et al., *Tectonics*, 2018

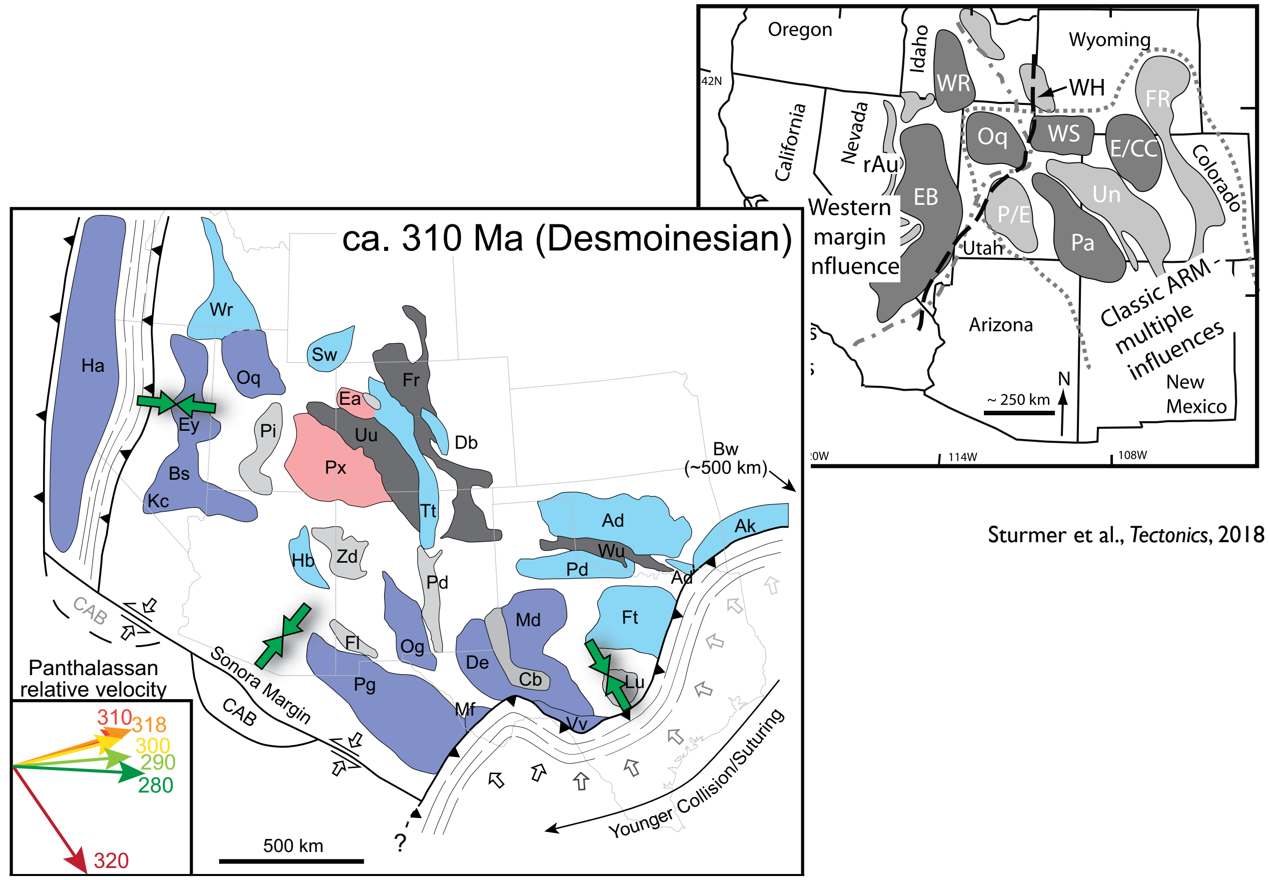

Sturmer et al., *Tectonics*, 2018

Leary et al., *Geology*, 2017

Both of these papers separate ARM from basins at western margin